Multidisciplinary Design Optimization of a Strut-Braced Wing Aircraft with Tip-Mounted Engines

By

J.M. Grasmeyer, A. Naghshineh-Pour, P.-A. Tetrault,

B. Grossman, R.T. Haftka,* R.K. Kapania,

W.H. Mason, and J.A. Schetz

MAD 98-01-01

January, 1998

Supported by the NASA Langley Research Center
under grant NAG1-1852

Multidisciplinary Analysis and Design Center for Advanced Vehicles
Department of Aerospace and Ocean Engineering
Virginia Polytechnic Institute and State University
Blacksburg, VA 24061-0203

* Department of Aerospace Engineering, Mechanics and Engineering Science, University of Florida, Gainesville, FL 32611-6250

Contents

List of Figures

List of Tables

1. Executive Summary

The objective of this study is to use Multidisciplinary Design Optimization (MDO) to investigate the use of truss-braced wing concepts in concert with other advanced technologies to obtain a significant improvement in the performance of transonic transport aircraft. The truss topology introduces several opportunities. A higher aspect ratio and decreased wing thickness can be achieved without an increase in wing weight relative to a cantilever wing. The reduction in thickness allows the wing sweep to be reduced without incurring a transonic wave drag penalty. The reduced wing sweep allows a larger percentage of the wing area to achieve natural laminar flow. Additionally, tip-mounted engines are used to reduce the induced drag. The MDO approach helps the designer achieve the best technology integration by making optimum trades between competing physical effects in the design space.

For this study we are using a mission profile similar to the Boeing 777-200IGW. The transport carries 305 passengers in mixed class seating with a cruise Mach number of 0.85 for a range of 7,380 nmi. Throughout the study we compare the performance of the optimum truss-braced configurations with a current technology cantilever design similar to the 777-200IGW and an advanced technology optimized cantilever design.

In the first year of research we developed the basic infrastructure for the MDO evaluation of this concept. A suite of approximate analysis tools was assembled into a complete, conceptual-level MDO code. A single-strut was initially chosen as the most basic representation of the truss-braced wing topology. Several single-strut configurations were optimized for minimum takeoff gross weight, using eighteen design variables and seven constraints.

Some thought was given to the judicious use of advanced concepts and technology. The study incorporates natural laminar flow and a novel structural concept to overcome the traditional problem of strut-braced wings: buckling of the strut. Other than that, tip-mounted engines have been incorporated, but the effects of allowing the engines to be located under the wing have also been studied. The configuration appears to be particularly robust and amenable to the inclusion of numerous other concepts and technologies. However, to reduce risk and development cost, we have not incorporated these other possibilities, *e.g.*, active load alleviation, porous wing concepts, *etc*.

The resulting MDO design features a wing with an aspect ratio of 10.3, a sweep of 27.3˚, and a significant reduction in the thickness-to-chord ratio from a comparable cantilever wing configuration. The optimum single-strut design achieves laminar flow over 32% of the wing area, and the strut is fully laminar. The preliminary studies have shown the following performance gains for the single-strut configuration relative to a

current technology baseline cantilever configuration and an advanced technology optimum cantilever configuration

Table 1-1: Improvements of the optimum strut-braced wing configuration relative to the current technology and advanced technology cantilever wing configurations

Measure of Effectiveness	Relative to Current Technology Baseline Cantilever Configuration	Relative to Advanced Technology Optimum Cantilever Configuration
Takeoff Gross Weight	-23%	-14%
Fuel Weight	-36%	-21%
Operational Empty Weight	-20%	-16%
Cruise L/D	30%	12%
Seat-Miles/Gallon	56%	26%

In addition to the MDO work, we have been conducting weekly brainstorming sessions to develop innovative, unconventional arch-braced and ellipse-braced concepts. A plastic solid model of one of the novel configurations was created using the *I-DEAS* solid modeling software and the rapid prototyping hardware at Virginia Tech. This capability will allow easy visualization of complex configurations in the future.

2. Introduction

The idea of using a truss-braced wing for a long-range, transonic transport aircraft was first proposed by Werner Pfenninger at Northrop in the early 1950s [1]. He continued this work on and off until his retirement from NASA Langley in the late 1980s. Other truss-braced wing studies have also been performed at NASA [2] and [3], Boeing [4], and Lockheed [5]. However, none of these studies have been performed using a Multidisciplinary Design Optimization (MDO) methodology.

Because of the tight coupling between structures and aerodynamics in the truss-braced wing design problem, an MDO approach is required to assess the true potential of the concept. In June of 1996, a small research team within Virginia Tech's Multidisciplinary Analysis and Design (MAD) Center for Advanced Vehicles was tasked by NASA Langley to perform a thorough feasibility study of transonic, truss-braced wing configurations using an MDO approach. This report summarizes the research performed through December of 1998.

3. Problem Statement

The goal of this research has been to apply the Multidisciplinary Design Optimization (MDO) methodology to the design of a transonic, truss-braced wing to evaluate the concept feasibility.

The truss-braced wing concept embraces several synergistic design features to obtain a significant increase in performance. Conceptually, the structural efficiency of the truss allows the span to increase without an increase in wing weight or thickness (they may actually decrease). The increased span reduces the induced drag, and a decrease in thickness reduces the transonic wave drag and allows the wing sweep to be reduced. The reduced wing sweep and the smaller chord Reynolds numbers encourage laminar flow, which reduces the parasite drag. Obtaining the most desirable trade-off between these effects requires the use of MDO.

The design also uses tip-mounted engines to obtain a reduction in induced drag, as some studies have suggested [6] and [7]. The tip-mounted engines also provide added inertia relief for the wing structure. Since the engines are located at the wingtips, an engine failure would create a very large yawing moment. To maintain equilibrium flight at the engine-out flight condition, circulation control is used on the vertical tail to increase its effectiveness. The circulation of the vertical tail airfoil can be controlled by blowing air through slots at the rear of an elliptical section, or by combining the slots with a deflecting flap for some redundancy. The air for blowing can be provided by the Auxiliary Power Unit (APU), which is already located in the tailcone. In a study of a

circulation control stern plane for submarine applications, Englar and Williams [8] have shown that section lift coefficients of 2.8 are possible with a 20% ellipse. In normal flight, a small amount of blowing could also be used to create zero drag, or even some thrust. The circulation control concept, together with a stability and control analysis is used to incorporate the engine-out condition explicitly as a constraint. The increment in the vertical tail lift curve is currently used as a design variable with an upper bound of 1.0. The present model does not impose a weight penalty for the circulation control mechanism. Future research will evaluate the weight penalty and power requirements for the required amount of circulation control.

Thrust vectoring with a third engine mounted at the base of the vertical tail was also investigated as a means to handle the engine-out condition. We found that the relatively small deflection angles allowed by thrust vectoring (15˚) were not sufficient to generate a large enough yawing moment. The extra weight, maintenance, cost, and complexity of the third engine also discouraged the use of thrust vectoring.

The buckling of the strut under the -1g load condition proved to be the critical structural challenge in the single-strut configuration. To address this issue we allow the strut to be inactive in compression, and we optimize the strut force at the critical maneuver load condition (see Section 4.2.2 for details). In the Phase II research, we will investigate multi-element truss configurations and arch-strut configurations to address the buckling problem. Load alleviation and the use of composite structures will also be evaluated.

The investigation of the wing-strut interference drag has been started in Phase I with a computational fluid dynamics (CFD) analysis of a Douglas wing-pylon-store configuration using a structured grid. In Phase II, an unstructured grid methodology is being used to evaluate the wing-pylon-store configuration and some representative strut-wing configurations. Results from the unstructured grid analysis will become available in Phase II.

The Phase I research did not impose aeroelastic constraints on the design. In Phase II, an aeroelastic analysis will be performed with NASTRAN, and aeroelastic constraints will eventually be added to the MDO code.

3.1. Mission Profile

The truss-braced wing concept is best suited to a long-range mission, where the increase in efficiency can be fully utilized. A typical mission profile of the Boeing 777-200IGW was selected as the design mission profile for this study. As shown in Figure 3-1, it has a range of 7,380 nmi at Mach 0.85 with 305 passengers in a three-class configuration. An additional 500 nmi of cruise was added to satisfy the reserve fuel requirements. Fixed

fuel fractions are used for warmup, taxi, takeoff, and climb, and the Breguet range equation is used for cruise.

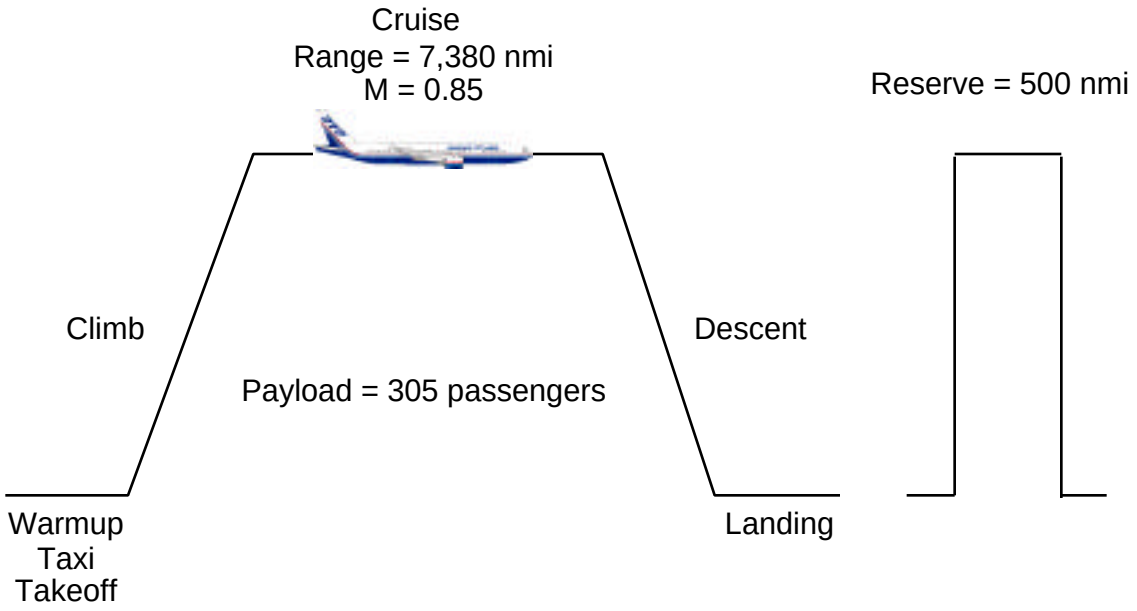

Figure 3-1: Boeing 777-200IGW mission profile

4. Approach

The main objective of the first year was to design and implement a multidisciplinary design optimization architecture capable of evaluating both cantilever and truss-braced configurations. A single-strut-braced configuration was chosen for the initial studies to establish the computational architecture and to gain a fundamental understanding of the design space. The Boeing 777-200IGW was chosen as the cantilever comparison aircraft.

4.1. Definition of the Optimization Problem

The objective of the truss-braced wing optimization problem is to minimize the takeoff gross weight of the configuration, subject to realistic constraints. The Design Optimization Tools (DOT) software from Vanderplatts is used to perform the optimizations with the method of feasible directions [9].

The single-strut-braced configuration is parameterized with the 18 design variables shown in Table 4-1. This includes 12 wing shape variables, such as span, sweep, *t/c* distribution, chord distribution, and the spanwise position of the wing-strut intersection. These are shown graphically in Figure 4-1. The vertical separation of the wing and strut at the root is specified to be equal to the fuselage diameter. The other 6 design variables

are the zero-fuel weight, fuel weight, cruise altitude, optimum strut force, the increase in the vertical tail lift coefficient due to circulation control, and the spanwise position of the engine. The fuselage and tail geometry of the Boeing 777-200IGW is used in all of the designs, and it remains fixed throughout the optimization. Six inequality constraints are used in the optimization to obtain realistic configurations, as shown in Table 4-2.

Table 4-1: Design variables

Number	Description
1	Spanwise position of wing-strut intersection
2	Semispan
3	Wing sweep
4	Strut sweep
5	Wing root chord
6	Wing chord at wing-strut intersection
7	Wing tip chord
8	Strut root chord
9	Strut tip chord
10	Wing inboard average *t/c*
11	Wing outboard average *t/c*
12	Strut *t/c*
13	Strut force
14	Vertical tail lift coefficient increment due to circulation control
15	Zero-fuel weight
16	Fuel weight
17	Spanwise position of engine
18	Average cruise altitude

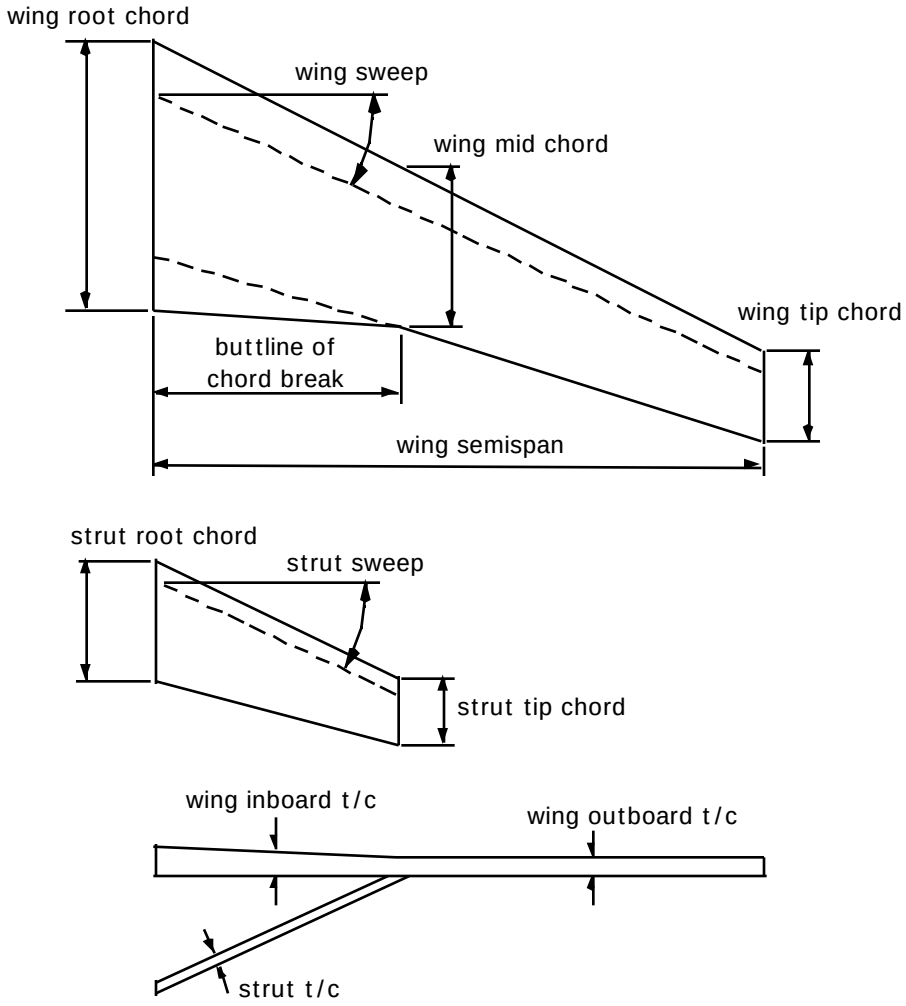

Figure 4-1: Wing geometry

Table 4-2: Constraints

Number	Description
1	Zero-fuel weight convergence
2	Range
3	Maximum aircraft lift coefficient at approach speed
4	Maximum allowable section lift coefficient at the beginning of cruise
5	Fuel volume
6	Engine-out
7	Wingtip deflection at the taxi bump load condition

The weight equations from NASA Langley's Flight Optimization System (FLOPS) are used to calculate most of the structural weight and all of the non-structural weight of the aircraft [10]. When using empirical weight equations, many of the aircraft structural components are sized based on an assumed takeoff gross weight. Therefore the calculated zero-fuel weight is a function of the initially assumed zero-fuel weight plus the fuel weight. In a traditional aircraft design methodology, an internal iteration loop is used to guarantee that the calculated zero-fuel weight is equal to the assumed zero-fuel weight. However, when an optimizer is already part of the code, it is more efficient to cast the zero-fuel weight and fuel weight as design variables, and use a constraint to enforce convergence [11].

The second constraint ensures that the aircraft range is greater than the range requirement specified in the design mission profile.

The third constraint ensures that the maximum aircraft lift coefficient at the approach speed is large enough to maintain equilibrium flight. The maximum lift coefficient of the unswept wing is assumed to be 3.3. The maximum lift coefficient of the swept wing is then calculated assuming a loss proportional to the cosine of the quarter-chord sweep angle.

The fourth constraint limits the maximum section lift coefficient at the initial cruise flight condition to be less 0.70. This prevents shock stall at high speeds.

The fifth constraint ensures that the fuel tanks have adequate capacity to carry the fuel required to fly the mission. The code has the capability to place extra fuel tanks in the fuselage outside of the wing carrythrough structure, but the optimum designs shown in this report do not require additional fuel capacity since this constraint is not active for them.

The engine-out constraint guarantees that the control system can achieve a sufficient yawing moment to maintain equilibrium flight after an engine failure at the minimum control speed defined by FAR 25.149.

The wingtip deflection constraint ensures that the wingtip or tip-mounted engine does not strike the ground during a taxi bump load. The current maximum allowable deflection is 25 ft., based on the fuselage height and landing gear length of the Boeing 777.

In addition to the inequality constraints mentioned above, side constraints are used to bound each design variable. The upper side constraint on the semispan design variable guarantees that the wing span is within the FAA 80 meter gate box limit. The lower side constraints on the wing and strut *t/c* design variables limit the minimum allowable wing and strut *t/c* values to 5%. The minimum *t/c* constraint has initially been arbitrarily specified, but it may be refined in the future when a more detailed systems analysis is performed.

4.2. Multidisciplinary Approach

Since the aerodynamics, structures, propulsion, and controls in the truss-braced wing problem are highly coupled, it is essential to use a multidisciplinary approach to assess the true potential of the configuration. Figure 4-2 shows the connectivity for the truss-braced wing design code architecture. This MDO tool integrates several analysis modules for aerodynamics, structures, and performance. The modular architecture allows for easy integration of higher-fidelity analysis modules, and it provides the capability to evaluate more complex truss topologies in the future.

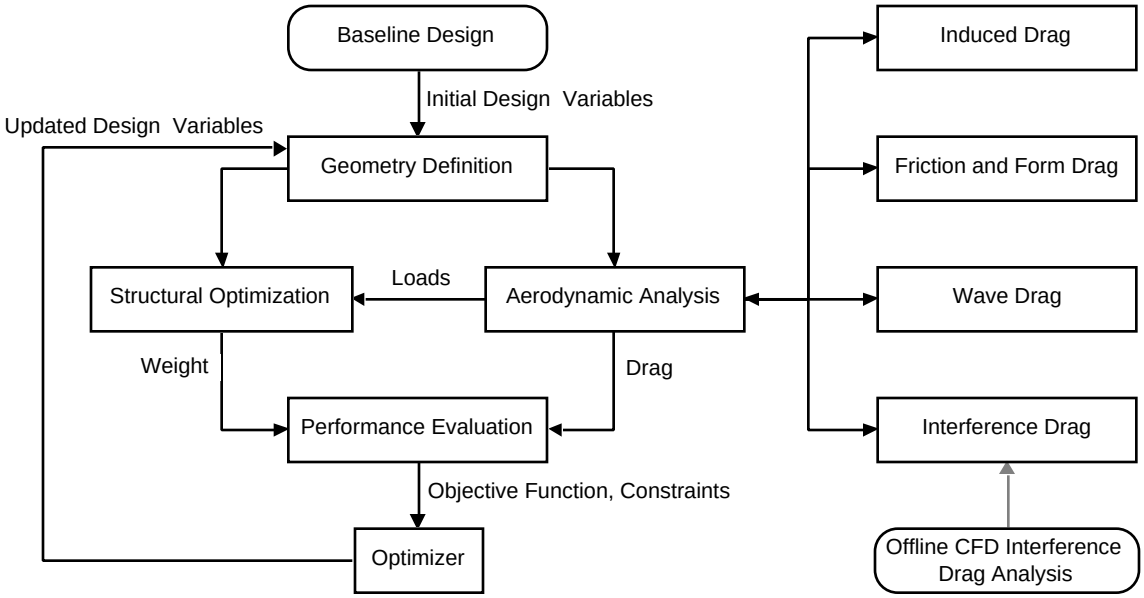

Figure 4-2: MDO code architecture

A brief overview of the aerodynamics, structures, and interference drag modules is given below. The complete documentation for the truss-braced wing design code can be found in Reference [12].

4.2.1. Aerodynamics, Stability and Control, and Propulsion

The aerodynamic performance is evaluated by modules for the induced drag, parasite drag, transonic wave drag, and interference drag. The stability and control derivatives are also estimated using a DATCOM-based method [13].

The induced drag module uses a discrete vortex method to calculate the induced drag in the Trefftz plane [14]. Given an arbitrary, noncoplanar wing/truss configuration, it provides the optimum load distribution corresponding to the minimum induced drag.*

* For our near-planar designs almost all of the load is carried by the wing.

Although the pitching moment about a specified center of gravity location can be specified, we did not impose a limitation on stability in this work.

Several studies have shown that the induced drag can be reduced by using tip-mounted engines [6] and [7]. Figure 4-3 shows the drag reduction as a function of the lift coefficient and aspect ratio, as given by Miranda and Brennan [7]. The MDO code uses a simple model based on this plot to approximate the induced drag reduction due to tip-mounted engines. Although the plot shows the total percent drag reduction, the percent reduction of the induced drag was determined and used in the MDO code. Notice that the aerodynamic advantage of tip-mounted engines gets smaller with increasing aspect ratio.

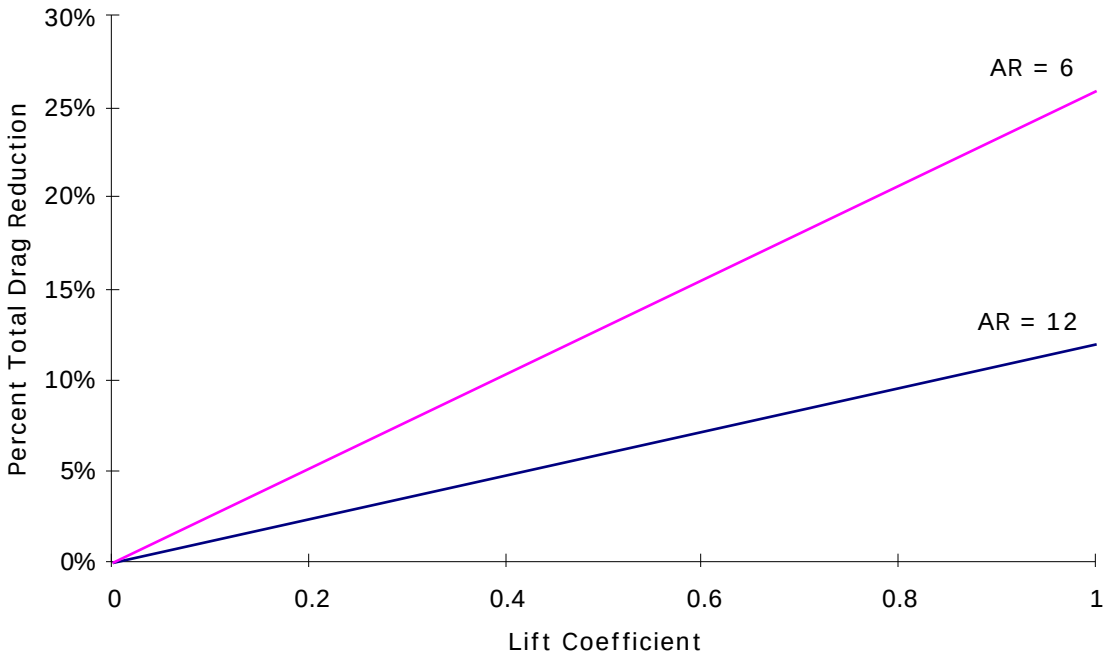

Figure 4-3: Drag reduction due to tip-mounted engines

To calculate the parasite drag, the amount of laminar flow is estimated using the transition Reynolds number vs. sweep data from Braslow and Collier [15]. The data for the F-14 and 757 glove experiments is shown in Figure 4-4. A laminar flow technology factor was added to the code to allow modification of the transition Reynolds number assumption. A value between zero and one is specified, where zero corresponds to the 757 glove experiment and one corresponds to the F-14 glove experiment. Skin friction formulas are then used with form factors to calculate the total parasite drag.

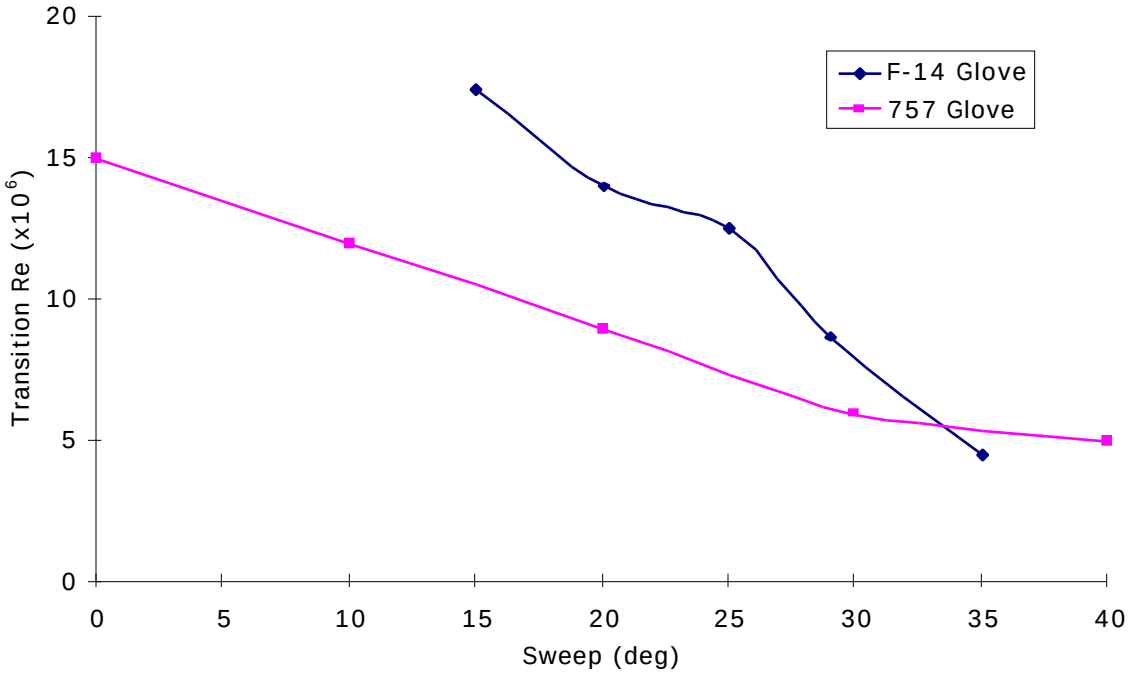

Figure 4-4: Transition Reynolds number vs. sweep

The transonic wave drag is approximated with the Korn equation, extended to include sweep using simple sweep theory [16]. This model estimates the drag divergence Mach number as a function of the local lift coefficient, thickness-to-chord ratio, sweep angle, and an airfoil technology factor. The wave drag coefficient is then calculated based on the definition of the critical Mach number, and Lock's empirically-derived exponential shape of the drag rise [17]. A number of strips are used across the span, and the total wave drag is the integrated contribution from each strip. This method has been validated with the Boeing 747-100, as shown in Figure 4-5. The solid lines represent the truss-braced-wing code results, and the discrete data points represent the Boeing 747 flight test data. The code predictions show good agreement with the data over a wide range of Mach numbers and lift coefficients. The results are sensitive to the value of the airfoil technology factor. A value of 0.89 was used for the Boeing 747 results in Figure 4-5. Based on our analysis of the Boeing 777, we used a value of 0.955 for the cantilever and strut-braced configurations presented in this report.

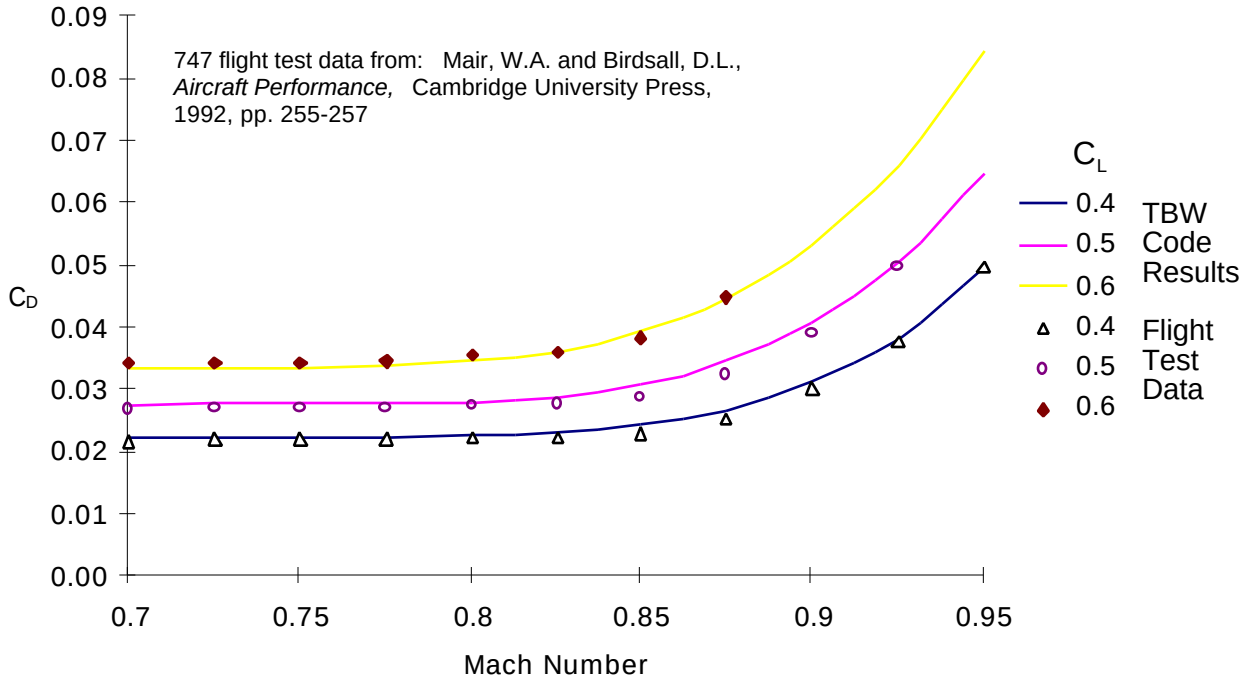

Figure 4-5: Boeing 747-100 drag rise comparison

The interference drag is currently estimated with the formulas given by Hoerner in *Fluid-Dynamic Drag* [18]. These empirical formulas were developed from low-speed experimental data. To determine the transonic interference drag effects we plan to use a response surface methodology to create an interference drag model from several detailed CFD analyses (see Section 4.2.3).

The use of tip-mounted engines requires careful attention to the engine-out analysis. The failure of a tip engine requires that the airframe produce a large yawing moment to maintain equilibrium flight at the engine-out flight condition. According to FAR 25.149, the aircraft is required to maintain steady flight with one failed outboard engine at 1.2 times the stall speed. The remaining outboard engine must be at the maximum available thrust, and the bank angle cannot be larger than 5˚. To enforce this constraint, we calculate the stability and control derivatives using the empirical method of Reference [19] (which is essentially DATCOM [13]). The available yawing moment is then calculated using a combination of rudder deflection, thrust vectoring, and circulation control. The details of this method are given in Reference [20].

The use of circulation control on the vertical tail allows the creation of a large sideforce at relatively low sideslip angles. It effectively shifts the lift curve up by an increment in the vertical tail lift coefficient. At this point in the study, the increment in the vertical tail lift coefficient is implemented as a design variable with an upper bound

of 1.0. Most tip-mounted engine configurations to date have required a change in the vertical tail lift coefficient of about 0.9. According to the data given by Englar and Williams [8], this appears to be feasible. Future research will identify the weight and power impacts of using circulation control. The current model assumes no weight penalty for the circulation control mechanism.

A simple rubber engine sizing methodology is used to scale the baseline engines to the required thrust. The rubber engine weight and nacelle drag are assumed to be linearly proportional to the thrust required at the initial cruise condition. The functional form of the thrust lapse as a function of Mach number and altitude is taken from equation 2.42 on p. 36 of Mattingly's *Aircraft Engine Design* [21]. The coefficients in the equation were adjusted using a nonlinear regression analysis with a GE-90-like engine deck provided by NASA Langley.

When this rubber engine sizing methodology is applied to the current technology baseline cantilever configuration, the required sea-level static thrust is 92,577 lb. This is slightly conservative, compared to the actual sea-level static thrust of 90,764 lb. (from the NASA engine deck).

4.2.2. Structures

The weight equations from NASA Langley's Flight Optimization System (FLOPS) are used to estimate most of the structural weight, and all of the non-structural weight [10]. Since FLOPS only uses an empirical correction factor to estimate the bending material weight of a strut-braced wing, a more detailed analysis method has been developed. The wing bending material weight is estimated with a piecewise linear beam model and substituted for the value in FLOPS [22]. Replacing the bending material weight from FLOPS with other estimates has been done in High Speed Civil Transport research at Virginia Tech for several years [11].

The bending material weight model idealizes the wing as a beam with properties varying along the span. Because the strut force and strut position are design variables, the beam can be treated as a statically determinate structure (even though it is not). This means that we can calculate the bending moment distribution by simple quadrature and calculate the required panel thickness directly, so that the structural optimization is very easy. This also will also allow us to calculate the optimum material distribution needed to meet the wingtip displacement constraint from a simple formula. This final step will be done in the remaining Phase II research.

Two maneuver load conditions (2.5 g and -1.0 g), and a 1.67 g taxi bump load condition are used to determine the wing bending material weight. Coster and Haftka [23] showed that for a truss-braced wing subjected to negative maneuvers a significant weight penalty is required to prevent the strut from buckling in the -1.0 g load case. They

compared the buckling weights of strut-braced wing configurations with those of truss-braced wing configurations to explore the effects of buckling on different configurations. The results revealed that using a truss would reduce the weight penalty by approximately 50%, which is still significant. Hence, to eliminate the weight penalty due to strut buckling a different design philosophy was adopted.

The strut is assumed to be inactive in compression during the -1.0 g maneuver load case and the 1.67 g taxi bump case. This could be done with a telescoping sleeve mechanism or a hinge arrangement. During positive g maneuvers, the strut is in tension. Since the wing is clamped to the fuselage, it acts as a cantilever beam in the negative load cases and as a strut-braced beam in the positive load cases. Moreover, the strut force at the 2.5 g load case is optimized to provide the minimum total wing bending material weight. On a typical optimum single-strut design, this means that the strut would first engage in tension at around 0.75 g. The optimum strut force at 2.5 g is less than the strut force that would be obtained at 2.5 g if the strut engaged immediately at 0 g (this could be thought of as the pre-force or jig-shape force). This design approach results in a significant reduction in the bending material weight compared to a wing in which a completely rigid strut is designed to withstand the buckling loads.

To reduce the axial forces on the strut a high-wing configuration is employed. The high wing puts the strut in tension for the 2.5 g load condition, making it much easier to cope with the buckling when it is limited to -1.0 g. Moreover, a high wing will avoid adverse transonic flow interference on the upper surface with a truss placed in the supersonic flow region.

In the preliminary studies of a truss-braced wing we direct our attention to only single-strut-braced wing configurations which are a special case within the general class of truss-braced wing configurations. We intend to evaluate more complicated truss-braced wing configurations in the future with more advanced modeling techniques such as the finite element method.

The parameterization scheme used for the current strut-braced wing studies is shown in Figure 4-1. The wing is assumed to be made of a high strength aluminum alloy. The wing box consists of upper and lower wing skins. The wing is subjected to lift distribution loads obtained from the aerodynamic analysis.

The structural analysis code has been validated to ensure the integrity of the results. The bending material weight computed from the piecewise linear beam model is compared with the bending weights given by Torenbeek [24] and FLOPS [10] for the Boeing 747-100. Figure 4-6 presents the comparison. It shows good agreement.

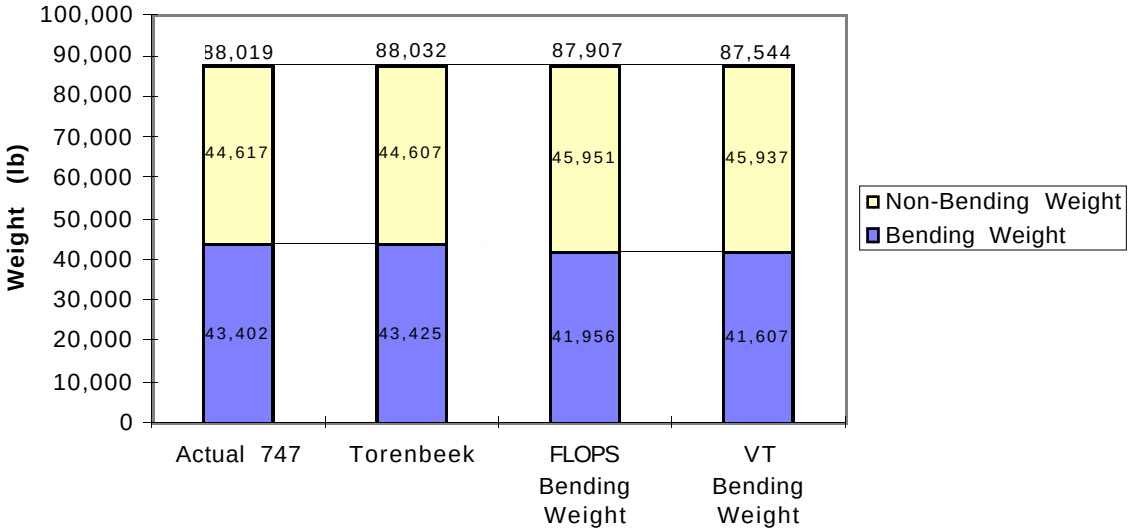

Figure 4-6: Bending material weight validation

Two sets of results will be shown in the plots below. The first set refers to the optimum strut-braced wing with tip-mounted engines and the second set refers to the optimum strut-braced wing with under-wing engines.

The shear force and bending moment distributions for the optimum single-strut design with tip-mounted engines are shown in Figure 4-7 and Figure 4-8, respectively.

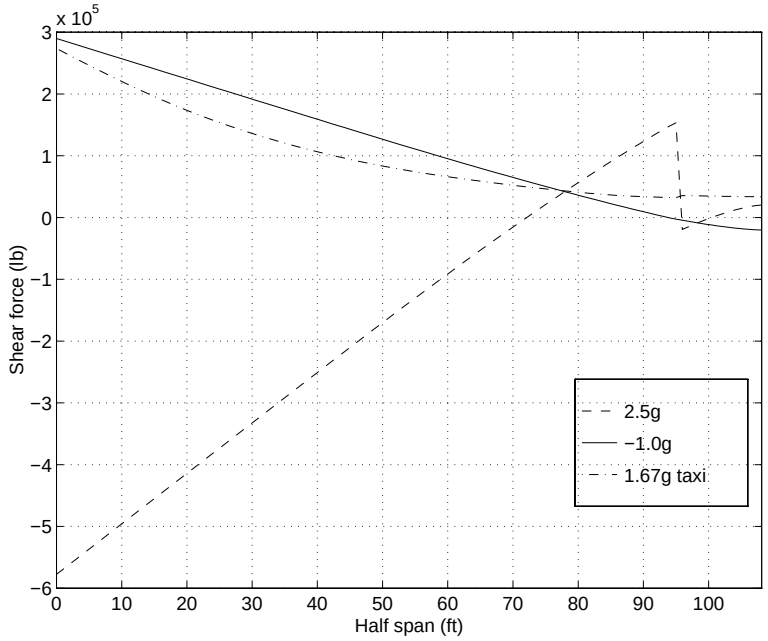

Figure 4-7: Shear force distribution for the single-strut design with tip engines

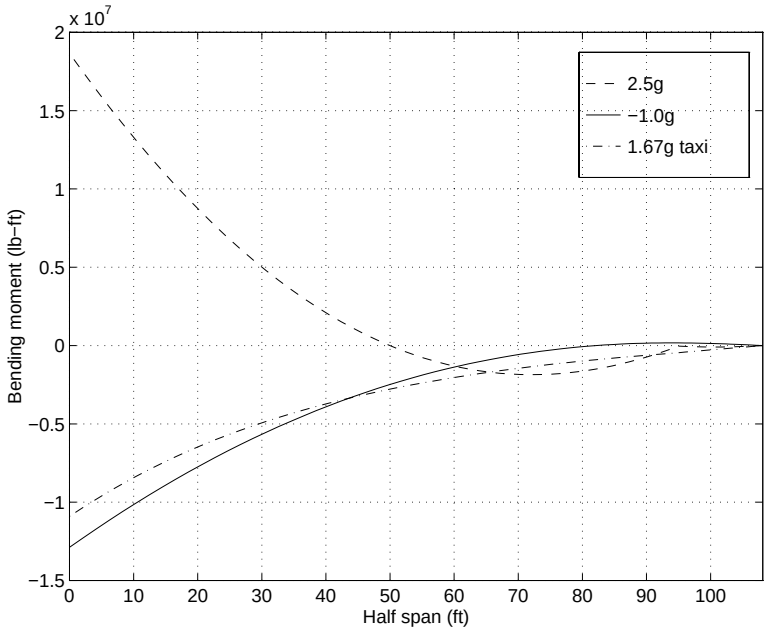

Figure 4-8: Bending moment distribution for the single-strut design with tip engines

The shear force and bending moment distributions for the optimum single-strut design with under-wing engines are shown in Figure 4-9 and Figure 4-10, respectively.

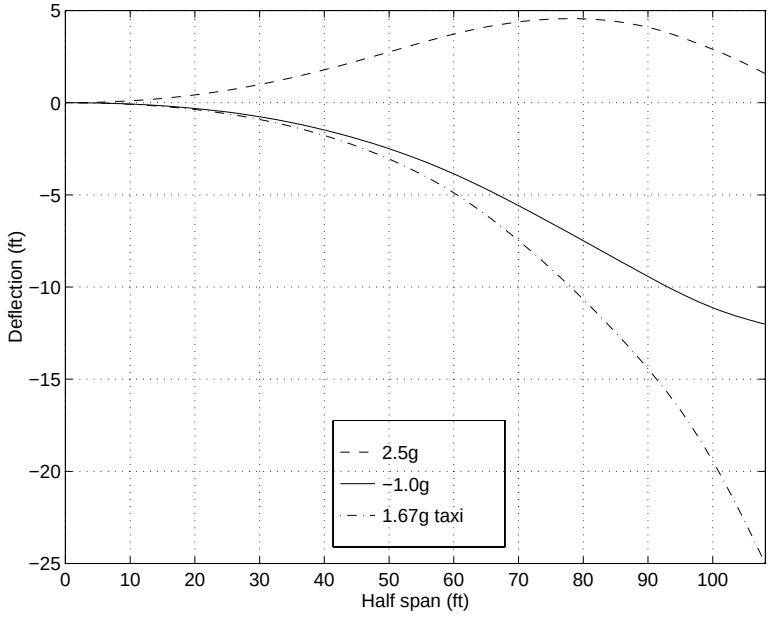

Figure 4-9: Shear force distribution for the single-strut design with under-wing engines

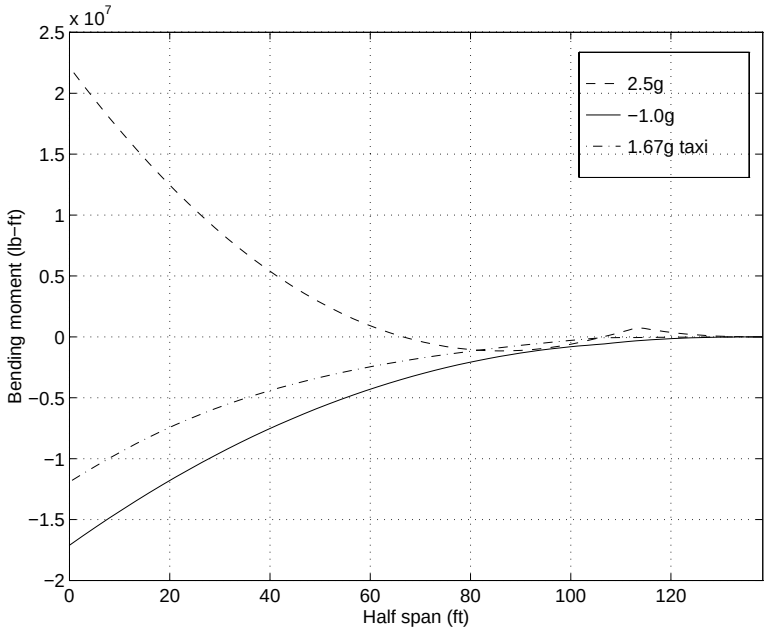

Figure 4-10: Bending moment distribution for the single-strut design with under-wing engines

The required wing box material thickness distributions for the tip-mounted and under-wing engine configurations are depicted in Figure 4-11 and Figure 4-12, respectively. The preliminary results showed an area of concern in the taxi condition where the required skin thickness distribution due to the taxi condition at certain wing locations may violate the required skin thickness distribution due to the maneuver conditions. This matter is taken care of by adding the required extra thickness due to the taxi condition at the aforementioned wing locations to the required thickness due to the maneuver conditions. A minimum gauge thickness of 0.004 ft. is used as a lower bound for the skin thickness distribution.

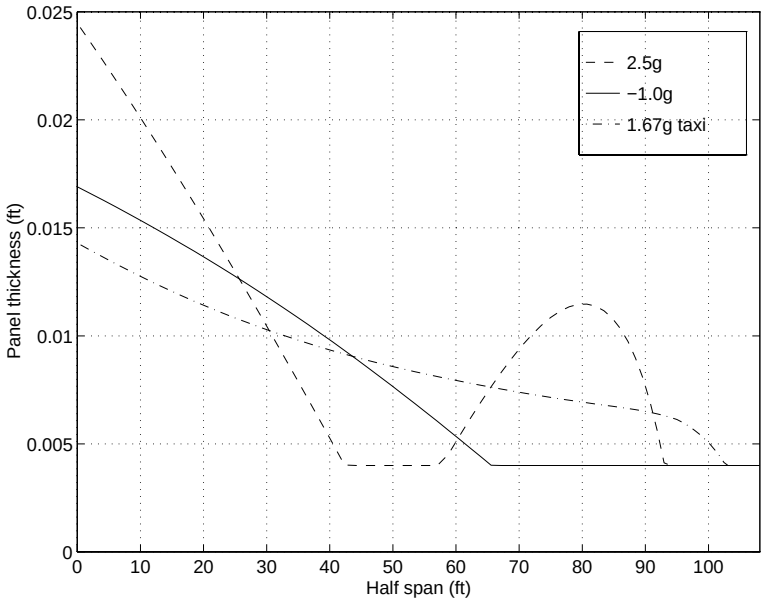

Figure 4-11: Structural material thickness distributions for the tip-mounted engine configuration

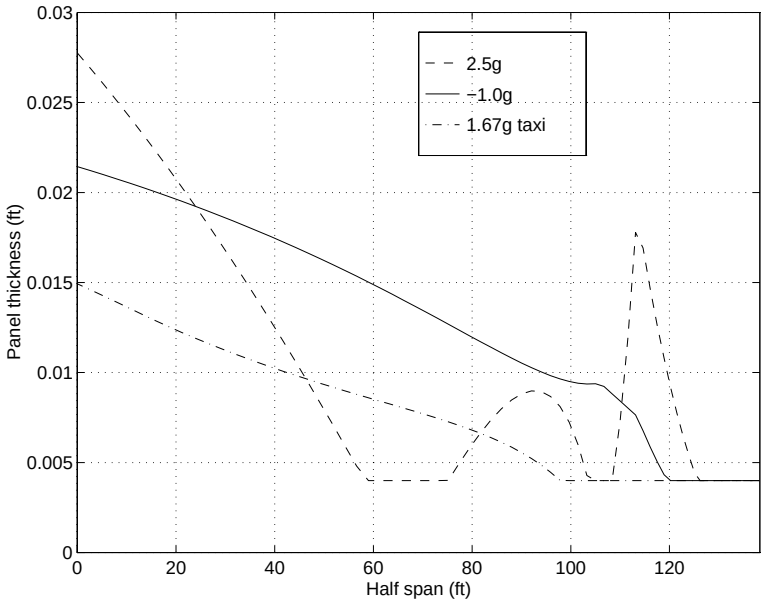

Figure 4-12: Structural material thickness distributions for the under-wing engine configuration

The skin thickness distribution plot shows that different load conditions determine the required panel thickness at different points along the span. Thus, for each spanwise station, the largest required thickness is used to calculate the wing bending material weight.

The vertical deflections for the maneuver and taxi bump load conditions are shown in Figure 4-13 and Figure 4-14. A maximum allowable wingtip deflection of 25 ft. is enforced at the taxi bump condition to prevent wing tip or engine ground strikes. The 25 ft. displacement limit was determined based on the fuselage diameter and the landing gear length. The displacement limit at the tip may require additional thickness at some points.

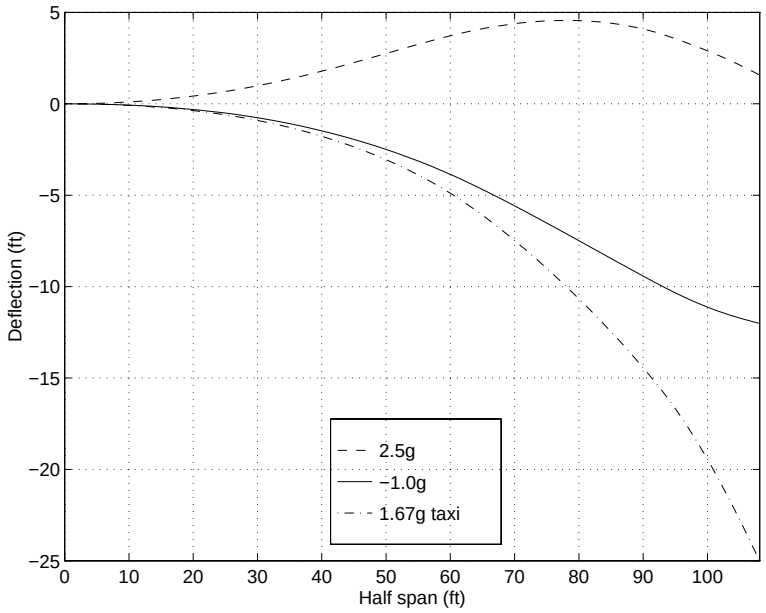

Figure 4-13: Deflections for the single-strut design with tip-mounted engines

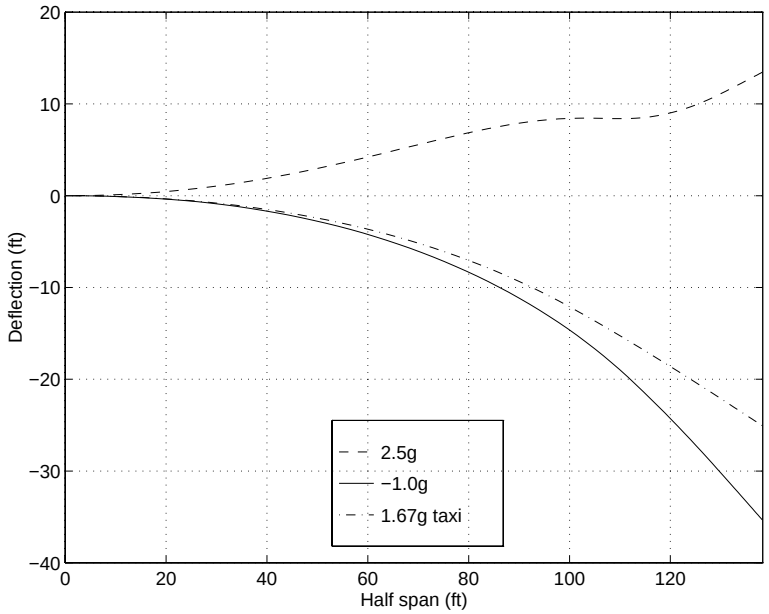

Figure 4-14: Deflections for the single-strut design with under-wing engines

The use of active load control has been investigated to understand the effects of load alleviation on potential bending material weight reduction. The aileron is used to shift approximately 10% of the lift inboard at the -1.0g condition. By deflecting the aileron, the wing intends to wash out at the tip, thereby shifting the lift inboard, as shown by Kulfan [25]. Hence, this phenomenon produces a bending weight reduction at the root since the lift centroid is also moved inboard. Preliminary studies showed that this mechanism could assist in achieving a significant reduction in bending material weight.

The current analysis method assumes a rigid wing when calculating the aerodynamic loads. In future research, the capability to model aeroelastic deflections will be added. The use of a flexible wing would naturally shift the load distribution inboard, since the swept wingtips would tend to wash out. Since the current design code does not model the effects of passive load alleviation, our current wing weight estimations are somewhat conservative.

During the remaining Phase II research, we will investigate the effects of composite materials on the strut-braced wing, use a finite element model methodology to evaluate more complicated truss-braced and arch-strut configurations, create a structural response surface model, and perform aeroelastic stability analyses.

4.2.3. Interference Drag

The development of a truss-braced wing aircraft is expected to lead to improved aerodynamic performance over a conventional cantilever wing design. However, the

estimation of the interference drag is a very important consideration in this type of design, especially in the transonic speed range where no detailed analysis has been performed in the literature. This drag penalty has to be assessed accurately in terms of the various design variables in order to include it in the MDO process.

To determine the effect of the geometry of the strut on the resulting drag coefficient, it was decided to use Computational Fluid Dynamics (CFD) tools. This approach allows us to analyze a broad range of configurations, from simple geometries such as a single strut design to more complex ones, such as an arch-shaped strut or a truss-braced wing aircraft. The effect of other ideas like the compression pylon and fillets can also be determined in a reasonable period of time.

As a first step towards that goal, structured grids were generated around a 2-D airfoil and a 3-D wing with GRIDGEN [26]. The CFD code GASP 3.0 [27] was then used to solve the Euler equations on those grids for M = 0.75 and $\alpha = 4^{\circ}$. For the 3-D wing case, the results were compared with wind tunnel test data from Douglas and Transonic Small Disturbance (TSD) calculations from Grumman [28]. Reasonable agreement with experimental data was obtained.

As the geometries get more complex, it becomes increasingly difficult to obtain a good structured grid. Even with the use of the multi-block capabilities of GRIDGEN, the grid quality suffers from the presence of stores and oblique struts. Also, a small variation of the design geometry can necessitate a whole new definition of the blocks and grid point distribution along each edge. This process can be time-consuming and the CFD results obtained may not be accurate enough because of this lack of flexibility in the grid generation.

The unstructured grid methodology can alleviate most of the problems related to complex geometries. Alterations of the original geometry can be incorporated easily and the grid topology is not tied to the concept of blocks. After the various patches have been defined over the geometry with GRIDTOOL [29], the unstructured grid generation is performed with the Advancing Front/Advancing Layers methodology (AFM/ALM) [30, [31, [32] implemented in the software VGRID [29, [33]. Both inviscid and viscous grids can be developed with this package. The CFD code USM3D [29, [34] is used to solve the Euler equations on the domain.

Both structured and unstructured grid methodologies were applied to the solution of the flowfield around a wing-pylon-store configuration for M = 0.75 and $\alpha = 4^{\circ}$. The unstructured grid at the wing root and the C_p contours are shown in Figure 4-15. For this geometry, we have experimental data from Douglas and numerical results from a TSD analysis done by Grumman.

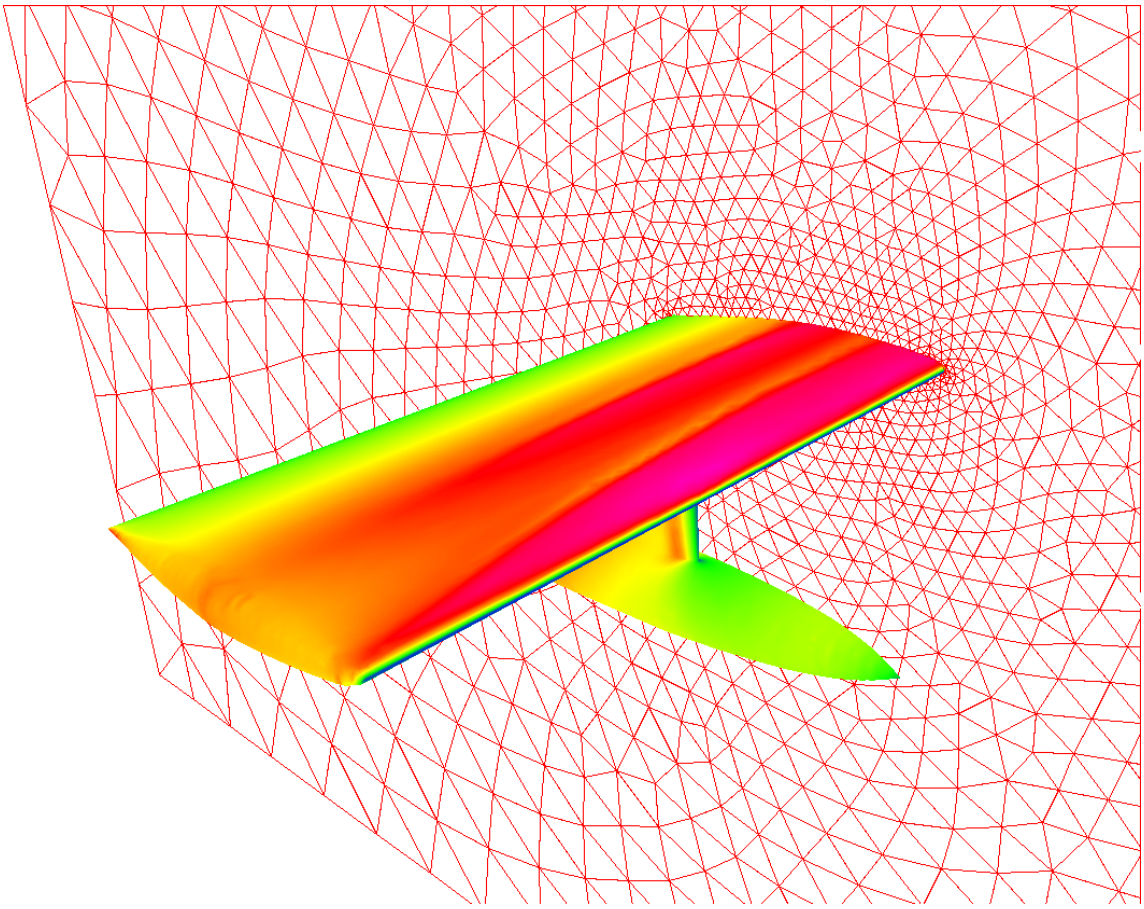

Figure 4-15: Grid and C_p contours for Douglas wing-pylon-store, M = 0.75, $\alpha = 4^\circ$

GASP 3.0 was used to solve the Euler equations on a structured grid. The C_p distribution at the pylon station is shown in Figure 4-16. The numerical results on the lower surface of the wing are represented by two curves: one for the inboard surface of the pylon and one for the outboard surface. The suction peak at the wing leading edge is overpredicted by our analysis. The predicted shock at mid-chord is not evident in the experimental data.

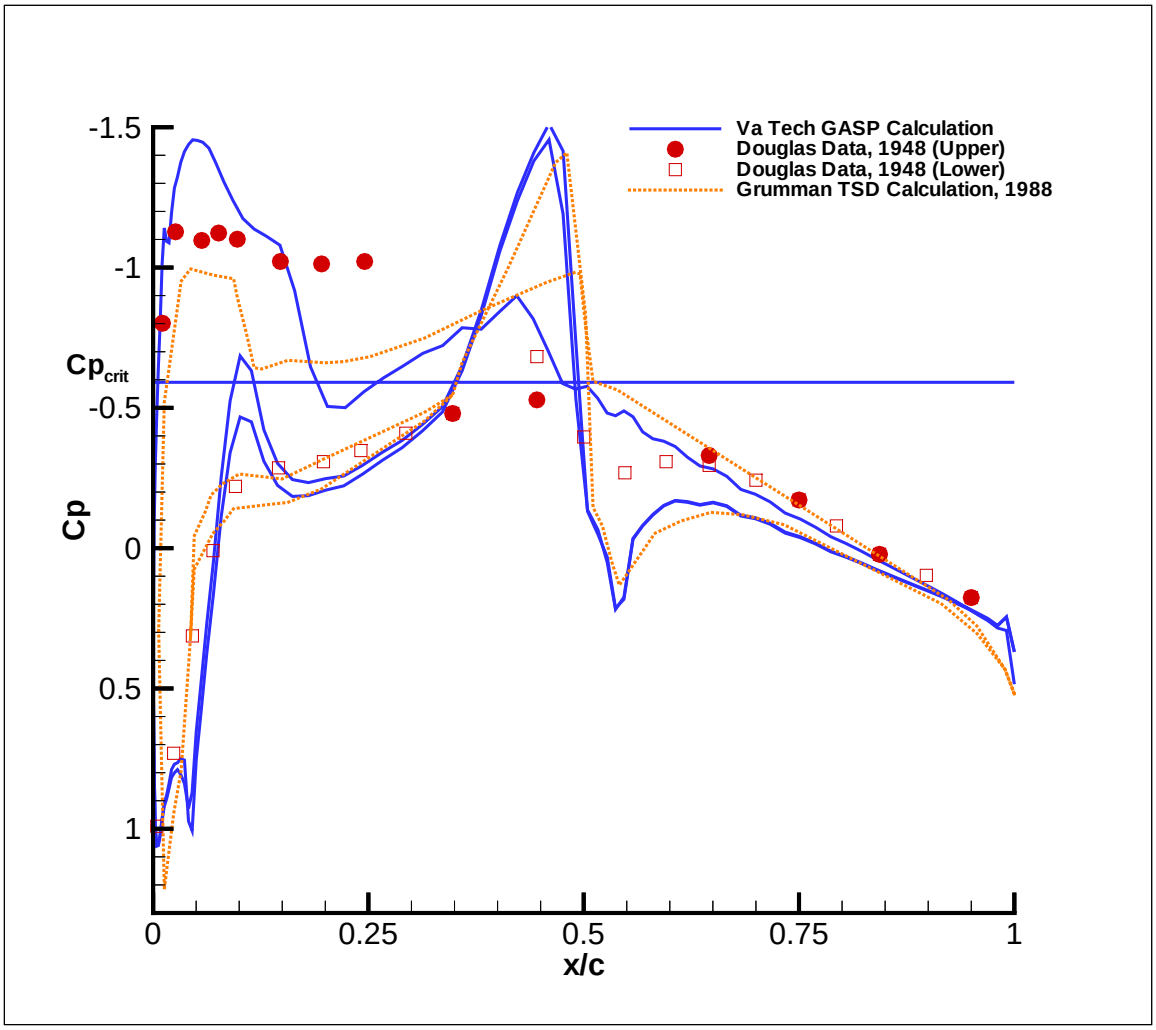

Figure 4-16: C_p distribution at the pylon station obtained with GASP, M = 0.75, $\alpha = 4^{\circ}$

The wing-pylon-store configuration was also analyzed on an unstructured grid with USM3D. The pressure coefficient at the pylon station is plotted in Figure 4-17. The CFD calculation agrees well with the data near the leading and trailing edges of the wing. The results are much closer to the experiment than the structured grid results were.

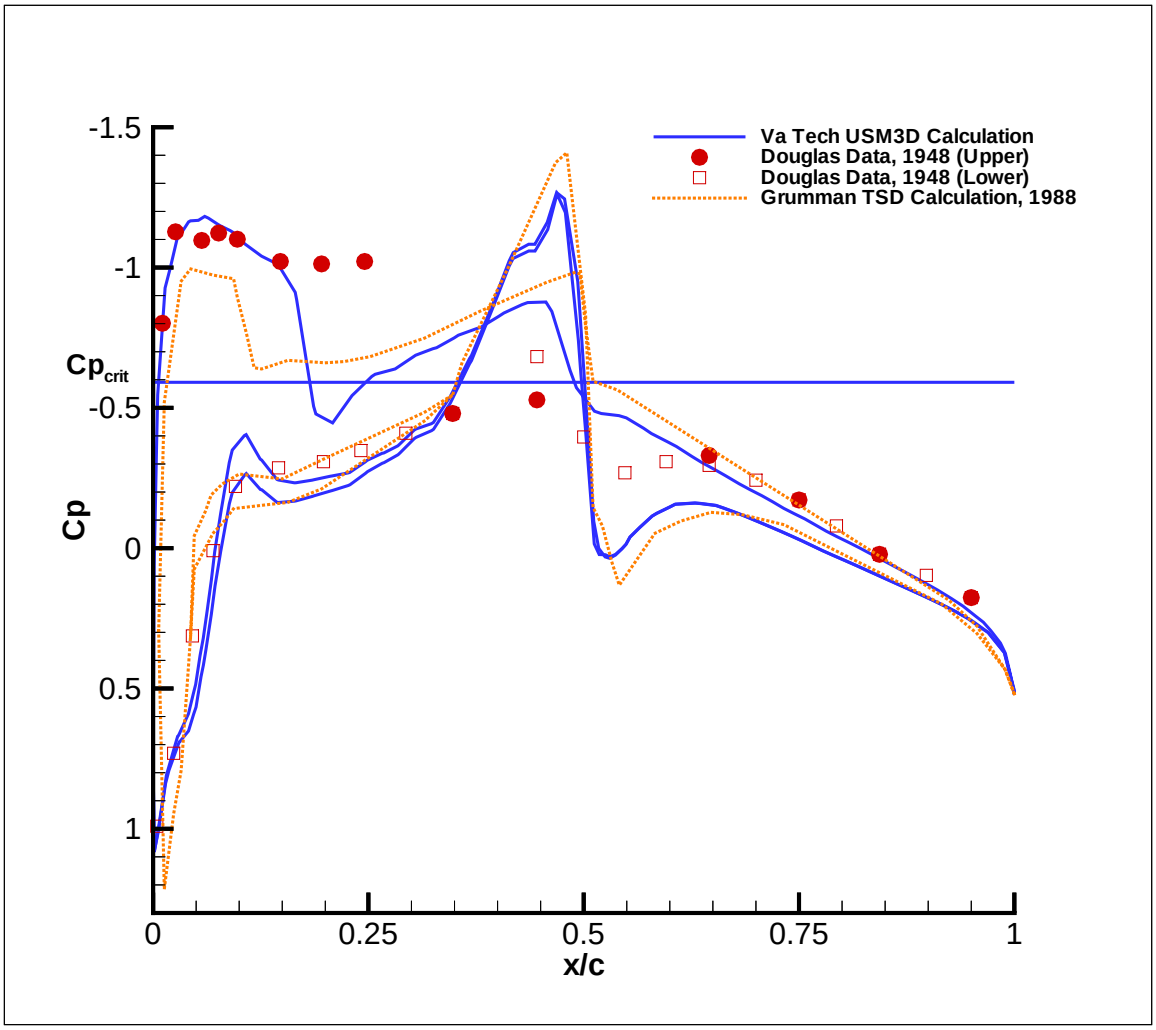

Figure 4-17: C_p distribution at the pylon station obtained with USM3D, M = 0.75, $\alpha = 4^\circ$

Recent efforts have focused on the application of the unstructured grid methodology to a single-strut design, using the same airfoil section as the other cases. The grid was developed for two representative configurations with 30˚ and 45˚ intersection angles between the wing and strut. Figure 4-18 shows the C_p contours and the unstructured grid for the 30˚ arrangement at M = 0.75 and $\alpha = 0^\circ$. Only a partially converged solution (1.5 orders of magnitude) could be obtained for both cases due to the presence of an unsteady flow region near the junction of the wing and the strut. This phenomenon was amplified for the 30˚ case since the gap between the wing and the strut was smaller in the vicinity of the intersection. To improve the quality of the flowfield in that region, it has been suggested to (1) use a thinner and smaller-chord airfoil section for the strut (2) make use of fillets in the junction to alleviate the effect of the sharp intersection, and (3) add sweep to the wing and strut.

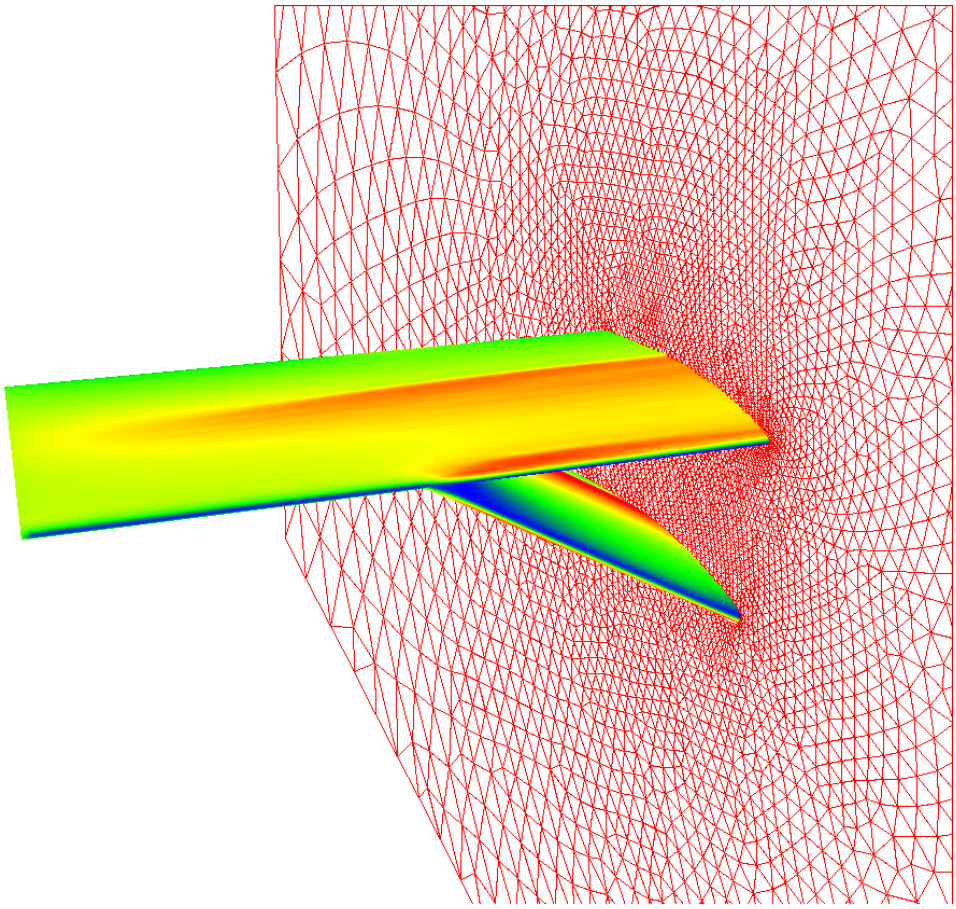

Figure 4-18: Grid and C_p contours for 30˚ wing-strut intersection, M = 0.75, α = 0˚

So far, the MDO methodology has produced several optimum single-strut designs. The analysis of the flowfield around one of these designs is underway. Supercritical airfoil sections have been selected and the geometry of the wing and the strut has been generated and is ready to be used with GRIDTOOL and VGRID. This step will bring us closer to generating realistic interference drag numbers and will help us understand the effect of the wing and strut design variables on the flowfield.

4.3. Validation

The design code was validated with the Boeing 747-100, the Boeing 777-200IGW, and a single-strut-braced military transport from a Boeing design study published in 1978 [25]. Each validation showed good agreement with the available weight, drag, and performance data. Our model of the Boeing 777 also compared favorably to a Boeing 777 model created by Matt Sexstone at NASA Langley [35].

5. Results

The goal of this study is to evaluate the feasibility of the truss-braced wing concept and compare the performance with the cantilever wing configuration, which has dominated the design of transonic transports since the advent of the Boeing 707. For this purpose, we have created two cantilever configurations to make such comparisons.

When performing an MDO study using relatively low fidelity analysis codes, it is important to validate the codes with a baseline configuration with known performance. For this study, we chose to validate the analysis codes with a representative model of the Boeing 777-200IGW. The weight and performance predicted by the MDO code were found to be in good agreement with the available data. This design is referred to as the current technology baseline cantilever configuration (Figure 5-1).

In the truss-braced wing MDO studies, we have introduced advanced technology concepts such as natural laminar flow and relaxed static stability to increase performance. We also use a rubber engine sizing method to match the engine size and weight to the required thrust, and several structural components are sized based on the takeoff gross weight. With these assumptions, the optimizer can redesign the baseline configuration to achieve the maximum benefit. It would be wrong to compare a truss-braced wing utilizing these assumptions and design degrees of freedom with a current technology cantilever design. Therefore, an advanced technology optimized cantilever configuration (Figure 5-2) was created by allowing the span, *t/c*, sweep, and chord distribution to be design variables and minimizing the takeoff gross weight. This configuration allows us to make valid comparisons between the cantilever and truss-braced wing concepts under the same set of technology assumptions, and using the same design methodology.

A single-strut-braced high wing configuration is currently used as the most basic representation of the truss-braced wing concept (Figure 5-3). Two variations on this concept are shown below. The first single-strut configuration was created by fixing the engines at the wingtips and optimizing seventeen design variables for minimum takeoff gross weight. The second configuration was created by allowing the spanwise position of the engines to be an additional design variable (Figure 5-4).*

As presented in Table 5-1, the advanced technology cantilever configuration shows a significant savings in takeoff gross weight due to the advanced technology assumptions, the design freedom provided by the design variables, the rubber engine sizing, and the sizing of several structural components based on the takeoff gross weight. The optimum single-strut design achieves a much larger savings in takeoff gross weight due to the

---

* We assume that the induced drag reduction due to tip-mounted engines is effective only when the engine is located exactly at the tip. If the engines were located at 99% of the span, no induced drag reduction would be calculated. For this reason, two single-strut optimizations were performed: one starting with the engines at the tip, and one starting with the engines partially inboard.

greater design freedom allowed by the strut, the increased structural efficiency of the strut, and the increase in laminar flow due to smaller chords and less sweep.

The following two sections will show the drag, weight, and cost comparisons between the four designs. The remaining sections will show the sensitivity of the optimum single-strut design with tip-mounted engines to changes in sweep, the amount of laminar flow, the airfoil technology, the wing-strut interference drag, and the design Mach number.

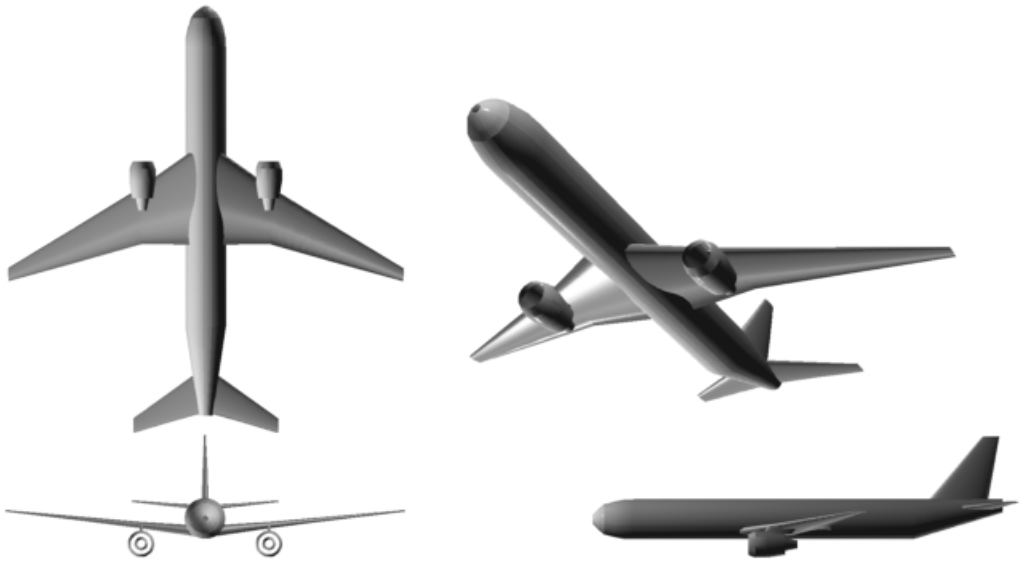

Figure 5-1: Current technology baseline cantilever configuration

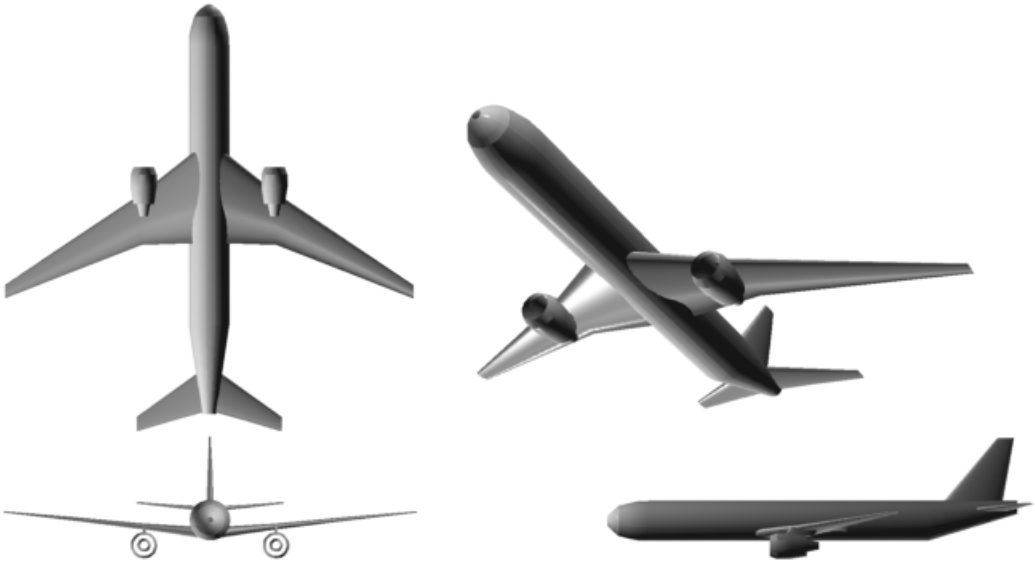

Figure 5-2: Advanced technology optimized cantilever configuration

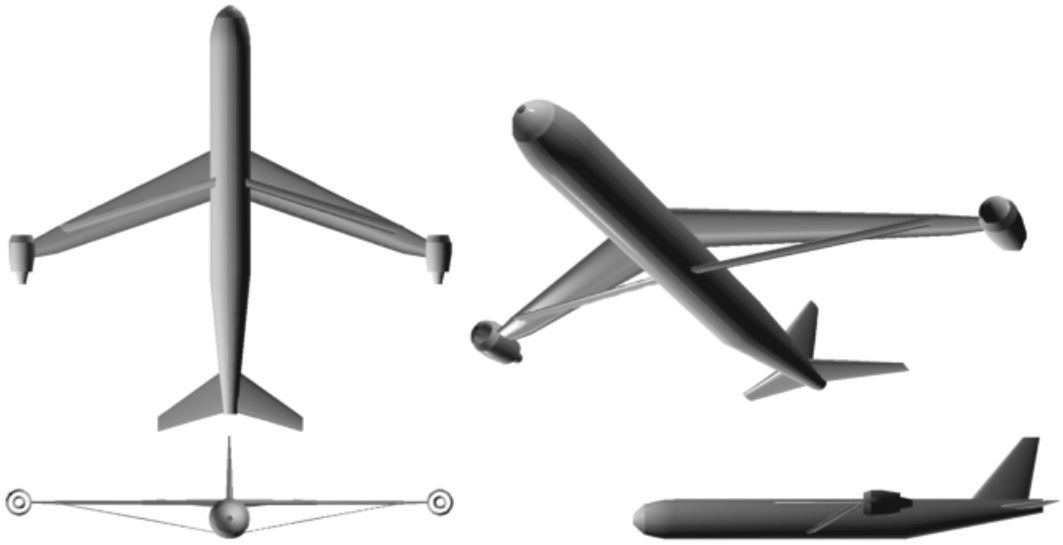

Figure 5-3: Optimum single-strut configuration with tip-mounted engines

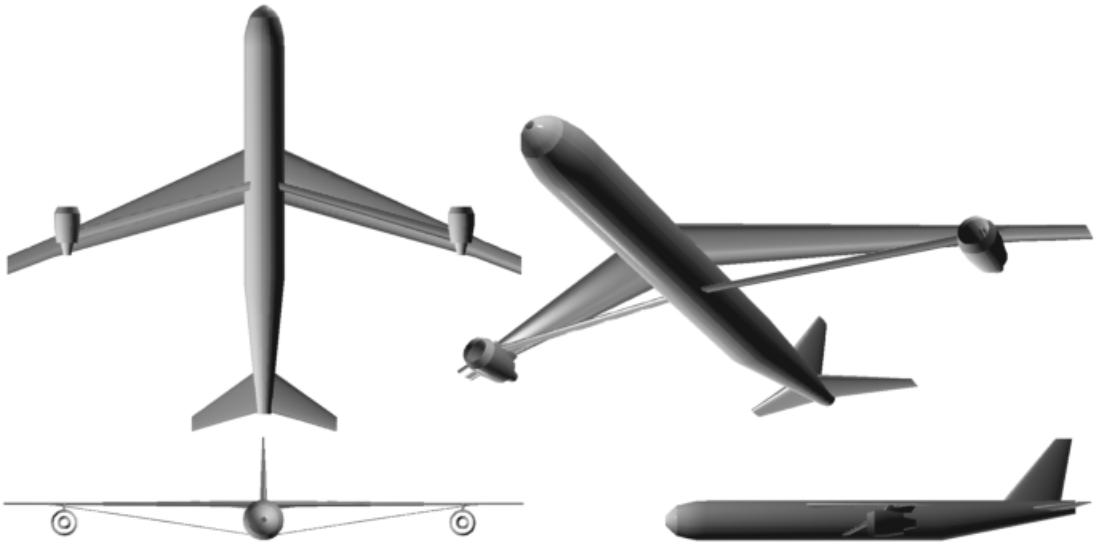

Figure 5-4: Optimum single-strut configuration with under-wing engines*

5.1. Comparison of Cantilever and Strut-Braced Designs

Table 5-1 shows a detailed comparison of the four configurations. The advanced technology optimized cantilever design shows a slight increase in span from the current technology cantilever configuration. The sweep also increased from 31.6˚ to 36.7˚ in

* Clearly the strut-pylon-nacelle integration details need to be resolved. Opportunities for additional drag reduction may arise when this is done.

order to reduce the wave drag. The *L/D* increased from 18.8 to 21.7, and the takeoff gross weight decreased from 632,081 lbs. to 568,031 lbs.

Table 5-1: Configuration comparison

	Current Technology Cantilever	Advanced Technology Cantilever	SS with Tip Engines	SS with Under-Wing Engines
Wing Span (ft)	199.9	206.6	198.9	258.7
Wing Area (ft2)	4,607	4,365	3,829	3,259
Aspect Ratio	8.7	9.8	10.3	20.5
Inboard Wing Sweep (deg)	31.6	36.7	27.3	24.5
Outboard Wing Sweep (deg)	31.6	36.7	27.3	24.5
Strut Sweep (deg)	N/A	N/A	17.7	16.3
Wing Root t/c	15.1%	15.4%	13.3%	11.9%
Wing Mid t/c	10.9%	10.5%	5.0%**	5.0%**
Wing Tip t/c	10.9%	10.5%	5.0%**	5.0%**
Strut t/c	N/A	N/A	5.0%**	5.0%**
Cruise L/D / Max L/D	18.8 / 20.9	21.7 / 24.0	24.4 / 27.4	27.8 / 31.5
Specific Range (nmi/1000 lb)	26.0	33.5	43.7	50.6
Seat Miles per Gallon (seats*nmi/gal)	60.5	74.7	94.2	105.2
Wing Weight (lb)	77,318	79,420	55,544	68,070
Takeoff Gross Weight (lb)	632,081	568,031	488,990	481,236

** The wing mid, tip, and strut *t/c* values have converged to the minimum allowable value of 5%.

The advanced technology cantilever design shows a 10% savings in takeoff gross weight relative to the current technology cantilever configuration. This weight savings is due in large part to the advanced technology assumptions such as partial laminar flow, relaxed static stability, and rubber engine sizing. The slight changes in the configuration also contributed to the weight savings.

Using the same technology assumptions and design methodology, the optimum single-strut design with tip-mounted engines achieves a weight savings of 23% relative to the current technology cantilever configuration. The wing weight is only 55,544 lb., even though the span is about the same as the current technology cantilever configuration. The sub-200 ft. span would allow this strut-braced design to operate in the same gates as the Boeing 747 and 777. The structural efficiency of the strut allows the *t/c* to be reduced to 13.3% at the root, and 5.0% outboard of the chord breakpoint (5% was chosen for the initial studies as the minimum allowable value for the *t/c*). The reduction in thickness allows the wing to unsweep to 27.3˚, and the strut has 17.7˚ of sweep. The result is an *L/D* of 24.4 and a takeoff gross weight of 488,990 lb. This is a 79,000 lb. reduction from

the advanced technology cantilever design, and a 143,000 lb. reduction from the current technology cantilever design.

The span of the single-strut design with tip-mounted engines was limited by the wingtip deflection constraint during the taxi bump load case.* A further increase in span would have caused the engines to strike the ground during a taxi bump. Therefore a second single-strut design was created with the spanwise position of the engine as an additional design variable. By moving the engine slightly inboard, the optimizer could increase the span to 258.7 ft., decrease the root *t/c* to 11.9%, and decrease the sweep to 24.5˚. These configuration changes resulted in an *L/D* of 27.8. The lower drag required less thrust, resulting in an 800 lb. weight savings on each engine, which further alleviated the tip strike constraint. The wing weight for this design increased to 68,070 lb., but the large fuel savings allowed the takeoff gross weight to decrease by about 7,000 lb. from the previous single-strut design. The FAA 80 meter gate box limit is equivalent to a wingspan of 262.5 ft. Therefore this design is barely within the maximum allowable gate box, which may present operational limitations on the design.

Note that the two single-strut configurations exploited two different modes for obtaining their low-weight. The tip-mounted engine design used the drag reduction available from mounting the engines at the tip to reduce the wing span and hence the wing weight. In contrast, the under-wing engine design obtained a lower fuel weight by significantly increasing the *L/D*. The induced drag was reduced by increasing the span, at the expense of a heavier wing. Increased laminar flow due to smaller chords and lower sweep also contribute to the low drag of this design. The resulting takeoff gross weights were very similar, with the under-wing engine configuration producing a slightly lower weight. This is a good example of how the MDO methodology can educate the designer about the nature of the design space, and discover synergisms that might be overlooked by using a more traditional design methodology. In this case, the designer might choose between the two configurations based on constraints that cannot be modeled mathematically.

The drag at the intersection of the strut and the engine pylon has not been calculated with a high-fidelity method. The existing drag model uses an empirical method to estimate the interference drag for the strut and the engine pylon separately, without considering their close proximity. Since the optimum spanwise position of the engines is at nearly the same buttline as the wing-strut intersection, a further drag reduction may be possible by creatively integrating the strut intersection with the engine nacelle and pylon. Future interference drag studies will address this issue.

---

* This constraint will be refined in future research by optimally allocating the required increase in skin thickness along the span.

Since the *t/c* of the outboard wing panel is only 5%, one would expect that a larger amount of laminar flow could be achieved on the outer panel by allowing it to have a sweep angle independent of the inboard panel sweep. This optimization was performed, and the resulting design has a wing with an inboard sweep of 26.9˚, and an outboard sweep of 19.3˚. The takeoff gross weight of this design is 476,717 lb, which is a 0.9% savings relative to the single-sweep design. Since the structural analysis does not model the additional weight and complexity that would be required at this discontinuous joint, the actual weight savings may be negligible, or the weight may actually increase.

5.2. Understanding the Optimum Configurations

To gain a better understanding of how the strut-braced wings achieves the dramatic increase in *L/D*, a comparison of the drag breakdown is shown in Figure 5-5. The absolute drag is shown because the reference areas are different, and the optimizer determines the optimum cruise altitude for each design, resulting in different dynamic pressures. The shaded bars show how the various components of the drag add up to form the total drag at the average cruise condition. Starting from the top, the bars represent the wing-strut interference drag, the wing-fuselage and strut-fuselage interference drag, the wave drag, the tail parasite drag, the strut parasite drag, the wing parasite drag, the total parasite drag of the engine nacelles, the fuselage parasite drag, and the induced drag. Note that the parasite drag of the fuselage and tails is nearly equal for the four designs, since only the wing geometry was allowed to change.

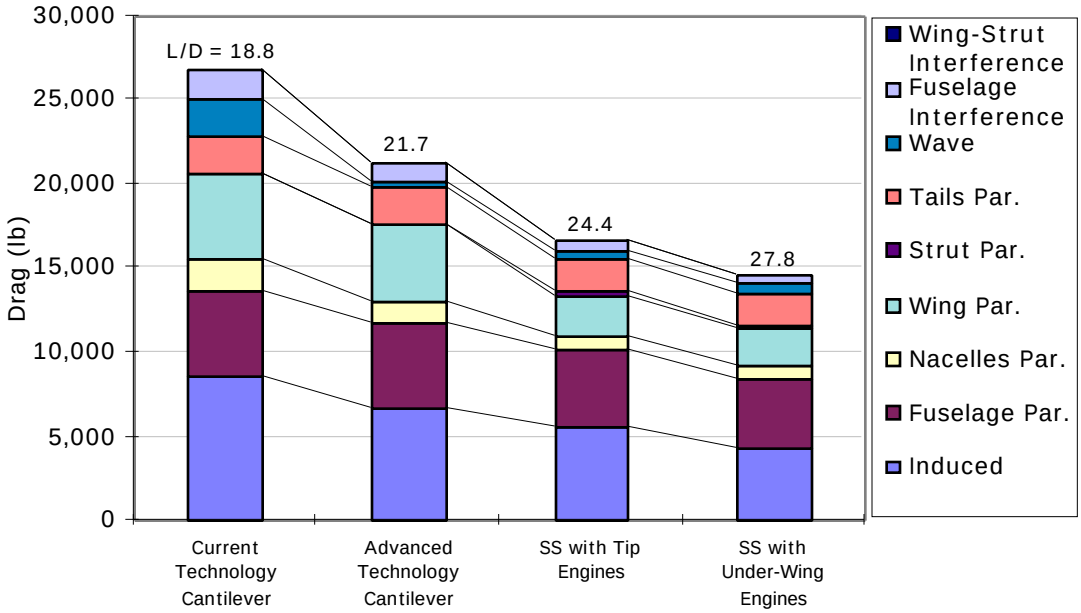

Figure 5-5: Drag comparison

The most dramatic change in drag for the advanced technology cantilever design is the reduction in induced drag due to the increase in span and decrease in weight and wing area. The average cruise lift coefficient decreased from 0.46 for the current technology configuration to 0.44 for the advanced technology configuration. The nacelle drag is somewhat smaller, since the higher *L/D* and lower weight of the optimum cantilever design reduce the required thrust, which results in smaller engines. The wing parasite drag actually decreased slightly, since 9.3% of the wing area became laminar. The wave drag was significantly reduced by the added sweep.

The optimum single-strut design with tip engines shows a further reduction in induced drag. The induced drag *coefficient* is actually slightly larger than the induced drag coefficient of the advanced technology cantilever design, but the large reduction in wing area resulted in a decrease in the *absolute* induced drag. The air density is also lower, since the optimum average cruise altitude increased from 35,987 ft. to 39,432 ft. The interaction of the tip-mounted engines with the wingtip vortex results in a 12.5% savings in induced drag, and a 4.9% savings in total drag for this design (relative to the same configuration with no induced drag reduction due to the tip engines). This drag savings would translate to a savings of 3.3% in takeoff gross weight.

Since the strut allows a smaller *t/c*, the wing can unsweep without a wave drag penalty. The reduction in sweep allows 31.9% of the wing area to become laminar. The strut also has some parasite drag, but since it has a small chord, and a low sweep angle, it is completely laminar and has very little drag.

The optimum single-strut design with under-wing engines shows the most significant reduction in induced drag, since the span increased to 258.7 ft. The smaller wing area and decreased air density due a further increase in altitude to 41,900 ft. also reduced the absolute drag. Further unsweeping of the wing to 24.5˚ results in 45.8% of the wing becoming laminar.

The interference drag is currently estimated using the low speed data and empirical equations presented in Hoerner's *Fluid-Dynamic Drag* [18]. The Hoerner data shows that the interference drag can be reduced with an increase in sweep. Since the advanced technology cantilever design has more sweep than the current technology cantilever design, the interference drag is lower, despite the increase in thickness.

The Hoerner data shows that the wing-fuselage interference drag is a function of $(t/c)^3$. Additionally, the drag coefficient is normalized by the chord squared over the reference area squared. Therefore a wing-fuselage intersection with a large *t/c* and large chord will have high interference drag, and an intersection with a small *t/c* and small chord will have low interference drag. Since the strut-braced wing has a smaller *t/c* and a much smaller wing root chord relative to the cantilever designs, it achieves a significant reduction in the wing-fuselage interference drag.

The main concern with the strut-braced wing has traditionally been the interference drag at the wing-strut intersection. However, since the average *t/c* and the average chord are both relatively small at the intersection, the interference drag is almost negligible. The reliability of this prediction is somewhat questionable, since the Hoerner data does not include transonic effects. Therefore, detailed CFD studies are being performed to locally shape the intersection geometry to avoid a large interference drag penalty (see Section 4.2.3).

Figure 5-6 shows the weight breakdown for the four designs. Starting from the top, the three shaded bars represent the fuel weight, the wing and strut weight, and the zero-fuel weight minus the weight of the wing and strut.

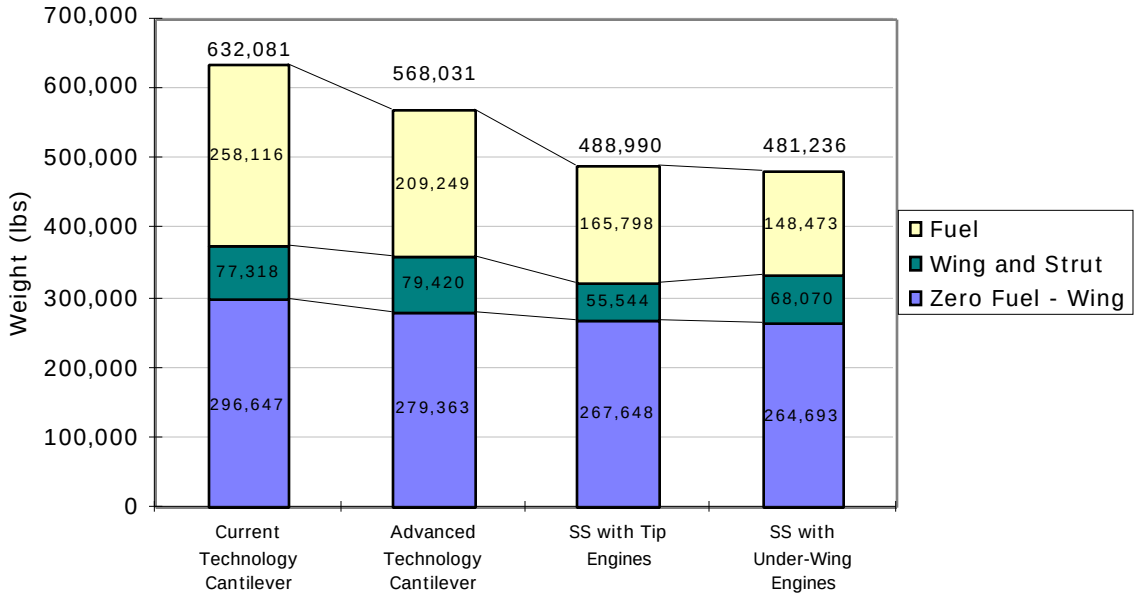

Figure 5-6: Weight comparison

Because of the increased cruise efficiency, the advanced technology cantilever design shows a 49,000 lb. fuel weight savings relative to the current technology configuration, and the optimum single-strut designs show a fuel weight savings of 92,000 lb. and 110,000 lb., respectively

The wing weight of the advanced technology cantilever design actually increased slightly due to the increase in span from 199.9 ft. to 206.6 ft. The strut-braced wing configurations achieved lower wing weights than the cantilever designs, even though the aspect ratios increased from 8.7 and 9.8 to 10.3 and 20.5. This counterintuitive result can be understood by looking at Figure 5-7. It shows the wing weight vs. aspect ratio for a series of cantilever and strut-braced configurations. The span was fixed for each design, and the rest of the design variables were optimized for minimum takeoff gross weight.

The rightmost point on each curve corresponds to a wing with a span of 262.5 ft., which is equivalent to the 80 meter gate box limit. The three curves represent a cantilever wing, a strut-braced wing with tip-mounted engines, and a strut-braced wing with under-wing engines at an optimum spanwise position. The strut-braced wings clearly pay a much smaller weight penalty for the increase in aspect ratio.

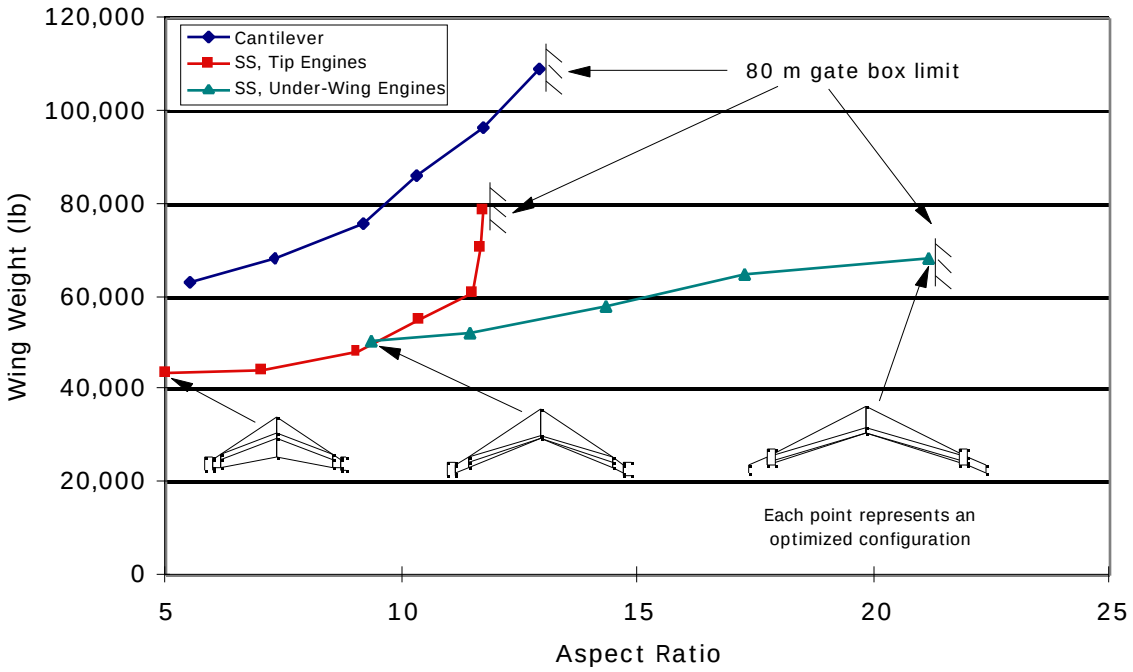

Figure 5-7: Wing weight vs. aspect ratio

Notice that the strut-braced wing curves in Figure 5-7 diverge at an aspect ratio of about 9.4. As the aspect ratio of the strut-braced wing with tip-mounted engines increases above this point, the wing weight increases rapidly since a significant amount of stiffness must be added to the wing to prevent the tip engines from striking the ground during a taxi bump. However, if the spanwise position of the engines is allowed to become a design variable, the engines tend to move inboard (thus sacrificing the induced drag reduction), and the span can increase without a large weight penalty. The upper bound for a strut-braced wing with under-wing engines is an aspect ratio of 21.1.

The cost breakdowns, shown in Figure 5-8, were estimated using the FLOPS cost model. Beginning from the top, the shaded bars represent the acquisition cost (AC), direct operating cost (DOC), and indirect operating cost (IOC). The costs are shown in year 2000 dollars. The fuel price was assumed to be $1.00 per gallon, and the airframe production quantity was assumed to be 1,000. A 30 year lifetime was used with a passenger load factor of 65%.

For this set of assumptions, the largest cost savings for the strut-braced wing configurations is seen in the direct operating cost (DOC). This is a result of the large fuel weight reduction due to the increased *L/D*.

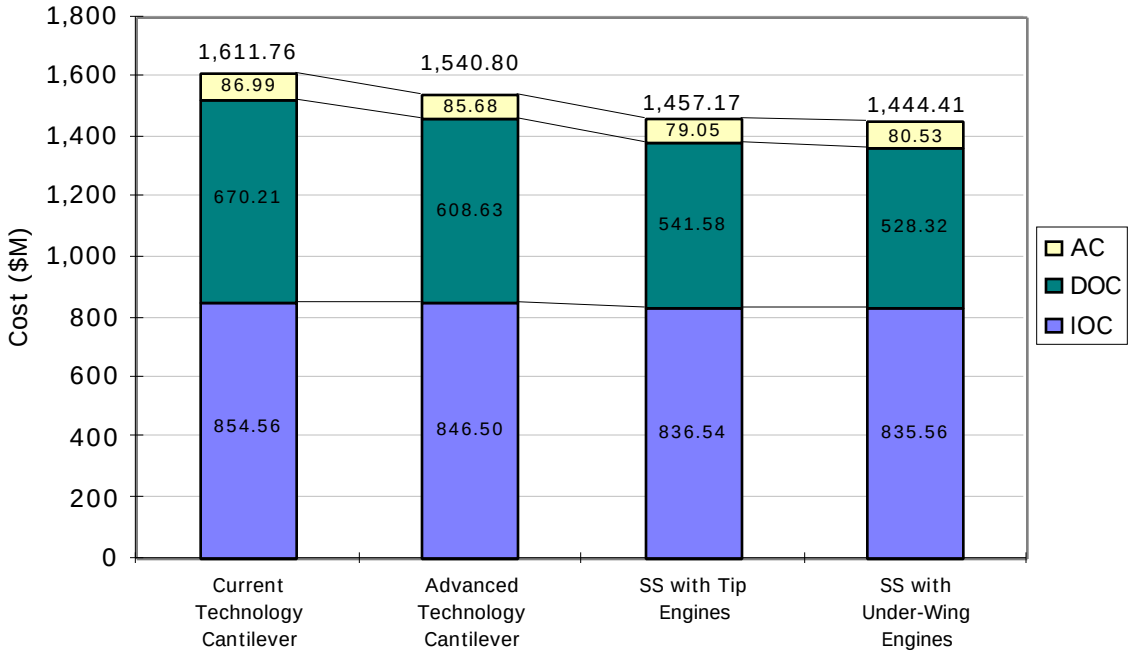

Figure 5-8: Cost comparison

5.3. Why is the sweep so high?

Since the amount of laminar flow decreases with increased sweep due to cross-flow instability, we initially expected the optimum strut-braced wing to be driven to a very low sweep angle to maximize the amount of laminar flow. However, the optimum design has a wing with a sweep of 27.3˚ (Figure 5-9).

To understand why the optimizer chose this sweep, two additional designs were created by forcing the wing and strut quarter-chord sweep angles to 50% of their original sweep (Figure 5-10), and to zero sweep (Figure 5-11). With the sweep angles fixed, the configurations were then optimized by allowing the rest of the design variables to remain free. The results are shown in Table 5-2.

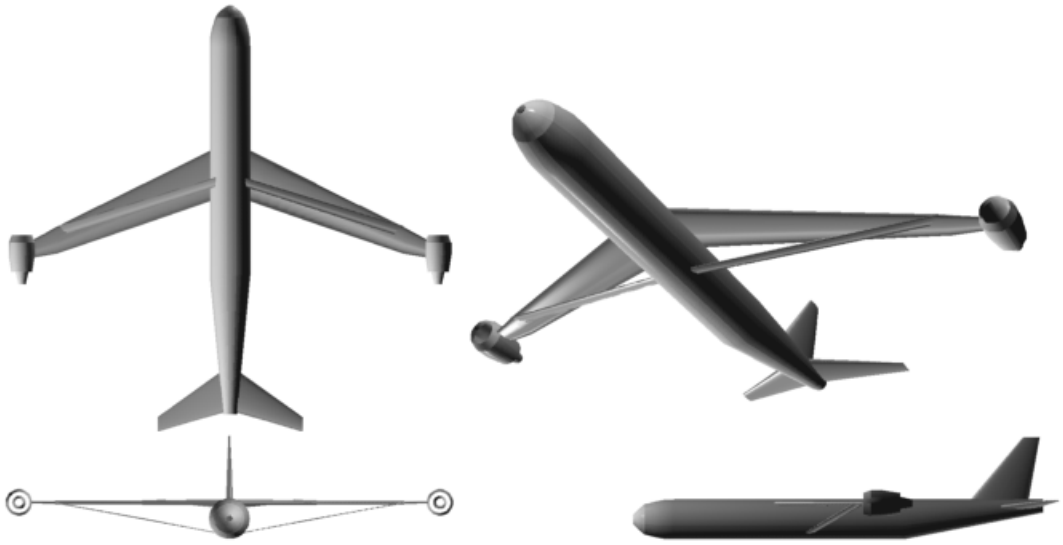

Figure 5-9: Original optimum single-strut configuration

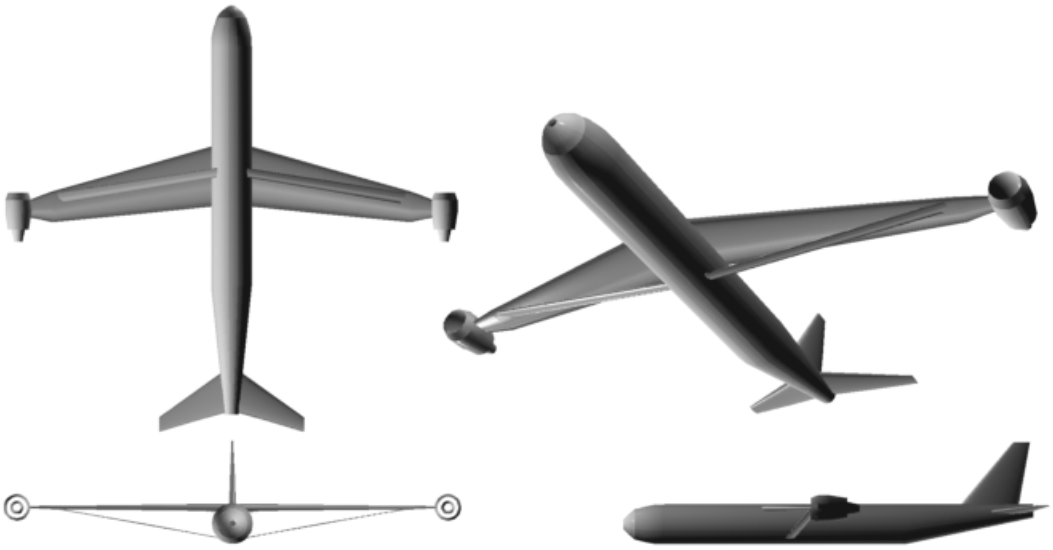

Figure 5-10: 50% sweep configuration

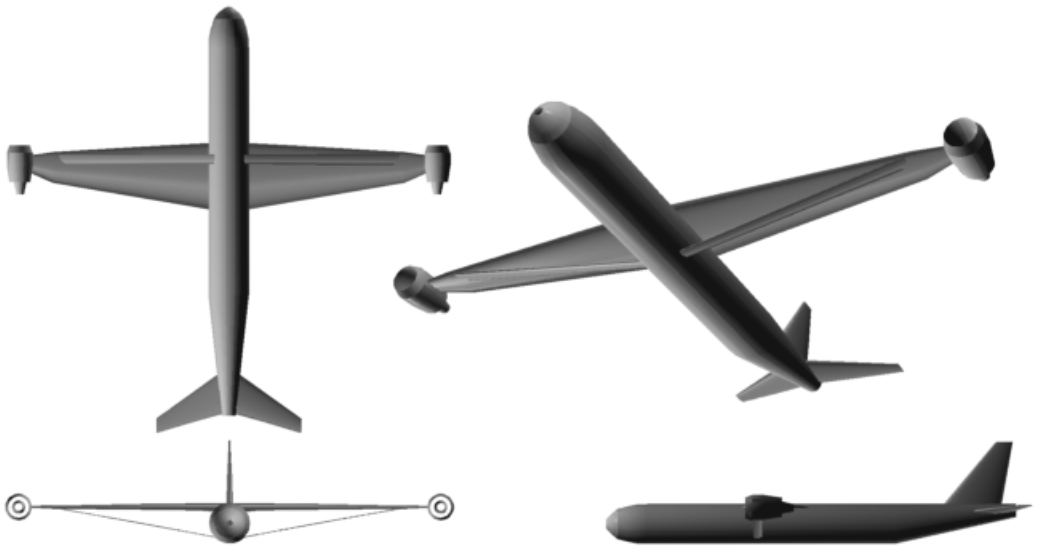

Figure 5-11: Fully unswept configuration

Table 5-2: Configuration comparison for unswept configurations

	Original Optimum Design	50% Sweep	No Sweep
Wing Span (ft)	198.9	203.9	199.5
Wing Area (ft2)	3,829	4,593	4,840
Aspect Ratio	10.3	9.1	8.2
Inboard Wing Sweep (deg)	27.3	13.7	0.0
Outboard Wing Sweep (deg)	27.3	13.7	0.0
Strut Sweep (deg)	17.7	8.9	0.0
Wing Root t/c	13.3%	10.1%	8.4%
Wing Mid t/c	5.0%**	5.0%**	5.0%**
Wing Tip t/c	5.0%**	5.0%**	5.0%**
Strut t/c	5.0%**	5.0%**	5.0%**
Cruise L/D / Max L/D	24.4 / 27.4	22.5 / 27.8	22.1 / 27.5
Specific Range (nmi/1000 lb)	43.7	37.6	36.3
Seat Miles per Gallon (seats*nmi/gal)	94.2	83.1	81.0
Wing Weight (lb)	55,544	61,788	63,645
Takeoff Gross Weight (lb)	488,990	522,409	530,206

** The wing mid, tip, and strut *t/c* values have converged to the minimum allowable value of 5%.

As the wing is forced to unsweep, the wing root *t/c* becomes smaller in an attempt to avoid a transonic wave drag penalty and a large interference drag penalty. As a result, the wing weight increases by 6,244 lbs. for the 50% sweep configuration, and by 8,101 lbs. for the fully unswept configuration.

Figure 5-12 presents the drag breakdown for the three configurations. As the wing is unswept, the amount of laminar flow on the wing increases from 31.9% on the original configuration to 46.6% and 59.8%, respectively for the unswept configurations. However, the large increase in required wing area reduces the savings in absolute parasite drag to a minimal amount. The most significant penalty for unsweeping the wing is the large increase in the wave drag.

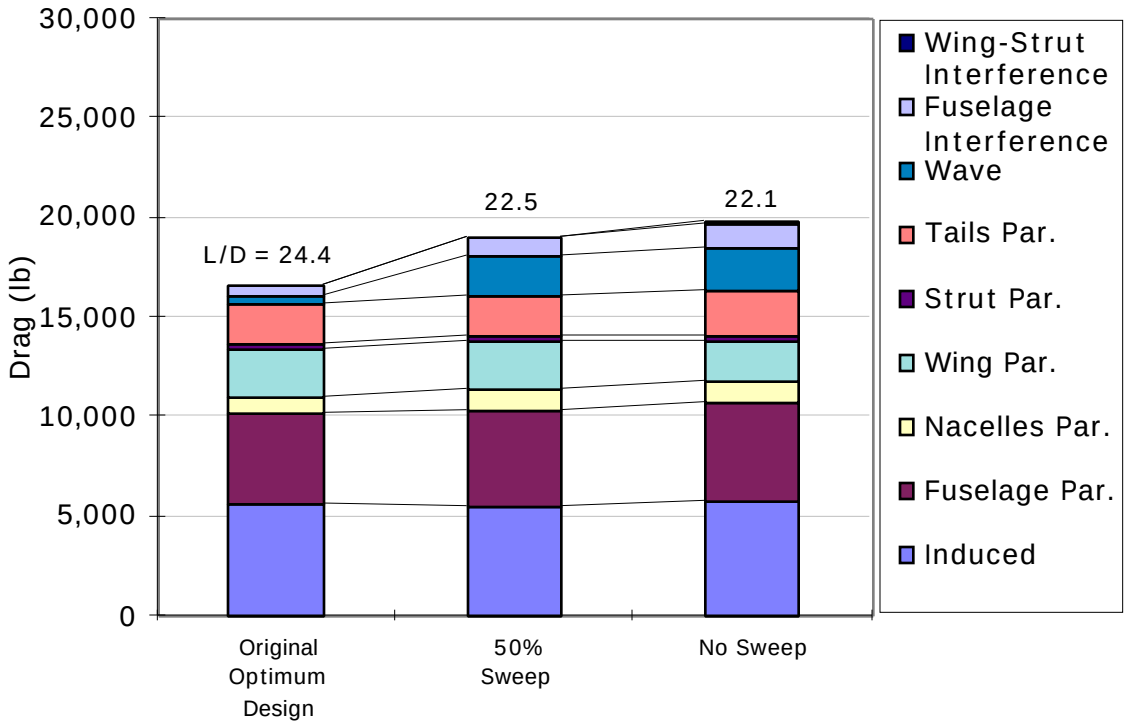

Figure 5-12: Drag comparison for unswept configurations

The weight breakdown is shown in Figure 5-13. The largest weight change is the weight growth of the wing due to the reduced *t/c* of the unswept configurations. The increase in wing weight requires a larger wing area, which results in more drag, which requires more fuel, which also requires more wing area, and so on. This is a classic example of how the ripple-through effect can amplify a small weight growth in one component into a significant increase in the takeoff gross weight.

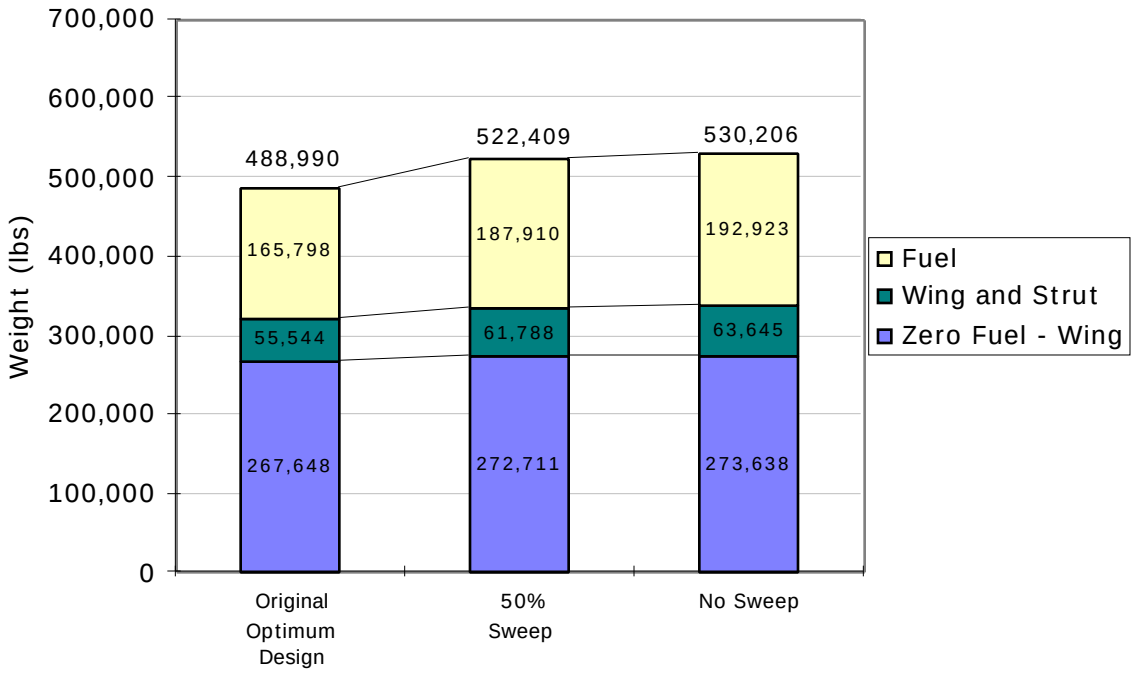

Figure 5-13: Weight comparison for unswept configurations

With the current assumptions and technology constraints, the optimum strut-braced wing configurations have sweep angles that are higher than our initial expectations. By creatively breaking down the traditional design constraints with advanced technology, the optimum wing sweep can be reduced, resulting in even greater performance.

For example, to avoid the rapid growth of wing weight with decreasing *t/c*, a load alleviation strategy could be used to shift the load distribution inboard at the critical load cases. To avoid the dramatic increase in wave drag with a decrease of sweep, a porous airfoil could be used to weaken the shock and improve the transonic drag rise characteristics.

This type of technology insertion study can be performed quite easily with the MDO code by changing a given technology level or modeling assumption, and re-optimizing the configuration to take maximum advantage of the change. The following sections will show sensitivities to the amount of laminar flow on the wing and strut, the airfoil technology, the wing-strut interference drag, and the design Mach number. The optimum single-strut design with tip-mounted engines is used as the baseline configuration for these studies.

5.4. Sensitivity to Laminar Flow

Figure 5-14 shows the amount of laminar flow on the optimum strut-braced configuration. The strut is displaced aft of the wing for the illustration, and the shaded areas represent the laminar flow regions. The configuration achieves 25% laminar flow near the wing root, 61% at the tip, and the strut is completely laminar.

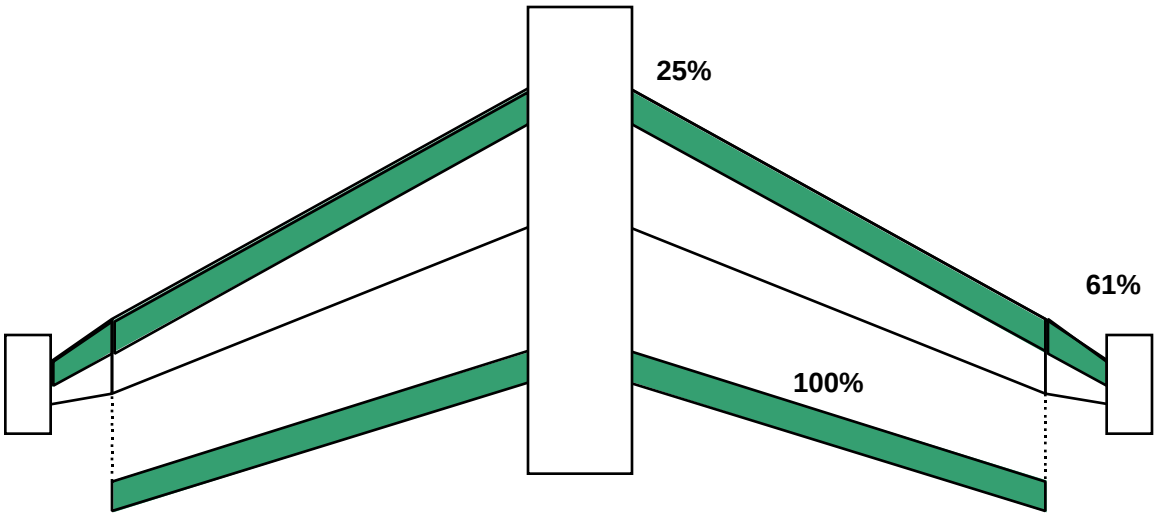

Figure 5-14: Laminar flow on optimum single-strut design (shaded regions are laminar)

Since laminar flow was originally perceived as the key to the success of the strut-braced configuration, a sensitivity study was performed with respect to the amount of laminar flow (Figure 5-15). The amount of laminar flow on the wing and strut was varied between 0% and 100% (by changing the transition Reynolds number), and the single-strut configuration was optimized for minimum takeoff gross weight at each point. About 32% of the wing area is laminar for the original optimum single-strut design. The change in takeoff gross weight between a fully turbulent wing/strut and a fully laminar wing/strut is about 104,000 lbs. The fuselage, nacelles, and tails are assumed to be fully turbulent, and represent 63% of the total wetted area for the advanced technology cantilever design, 62% for the single-strut design with tip-mounted engines, and 58% for the single-strut design with under-wing engines.

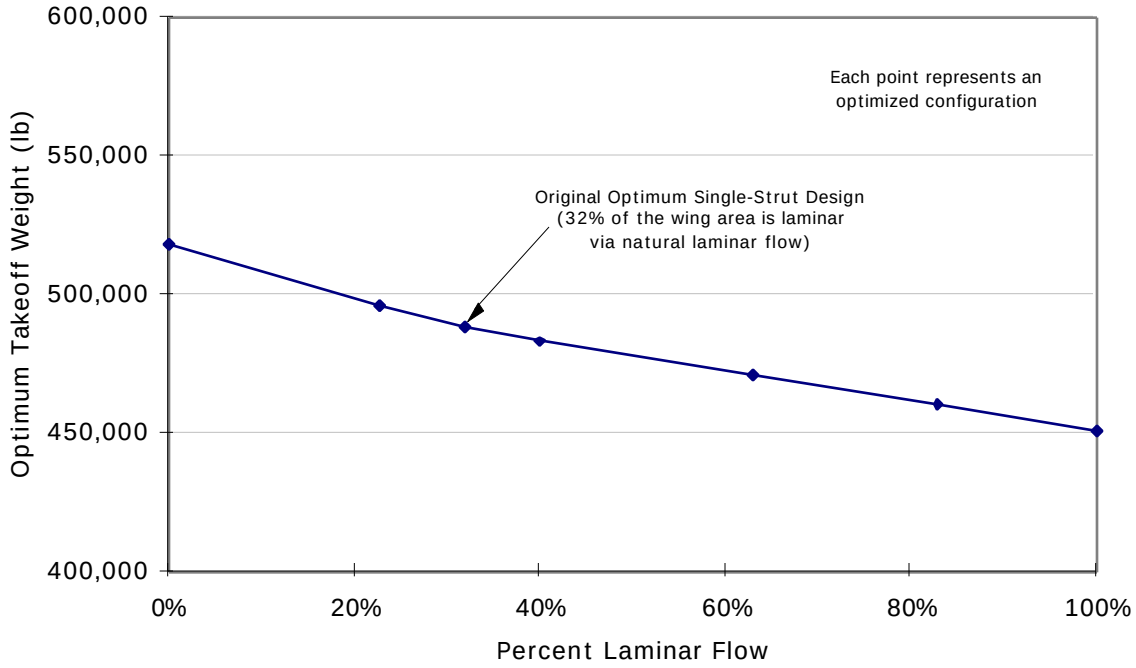

Figure 5-15: Sensitivity of the single-strut design to the amount of laminar flow

5.5. Sensitivity to the Airfoil Technology Factor

The shape and performance of the optimum wing design is very sensitive to the airfoil technology. The airfoil technology is modeled in the MDO code by the airfoil technology factor used in the Korn equation [16]. A value of 0.87 corresponds to a NACA 6-series airfoil section, while a value of 0.95 corresponds to a supercritical section.

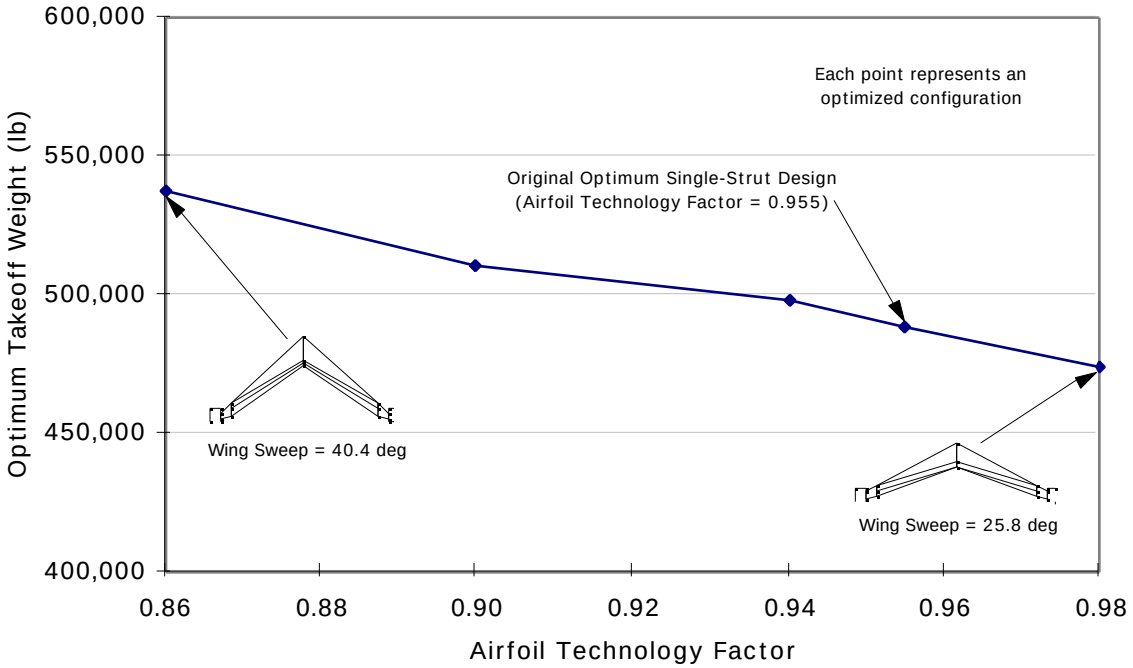

Figure 5-16: Sensitivity to the airfoil technology factor

The airfoil technology factor was swept from 0.86 to 0.98. Since the higher technology airfoils have better drag rise characteristics, the wing tends to unsweep with increasing airfoil technology. This study shows that changing the airfoil from a NACA 6-series section to a supercritical section would result in a weight savings of about 40,000 lb.

5.6. Sensitivity to the Wing-Strut Interference Drag

Since the interference drag calculations are based on the low-speed Hoerner data, the accuracy of the wing-strut interference drag requires more detailed analysis. To evaluate the impact of a potential increase in the wing-strut interference drag, a sensitivity study was performed by multiplying the Hoerner-predicted wing-strut interference drag by various amounts (Figure 5-17). Even when the Hoerner prediction is multiplied by a factor of 100, the takeoff gross weight only increases by about 27,700 lbs. The accuracy of this prediction will be improved in the future by creating a response surface from detailed CFD calculations (see section 4.2.3).

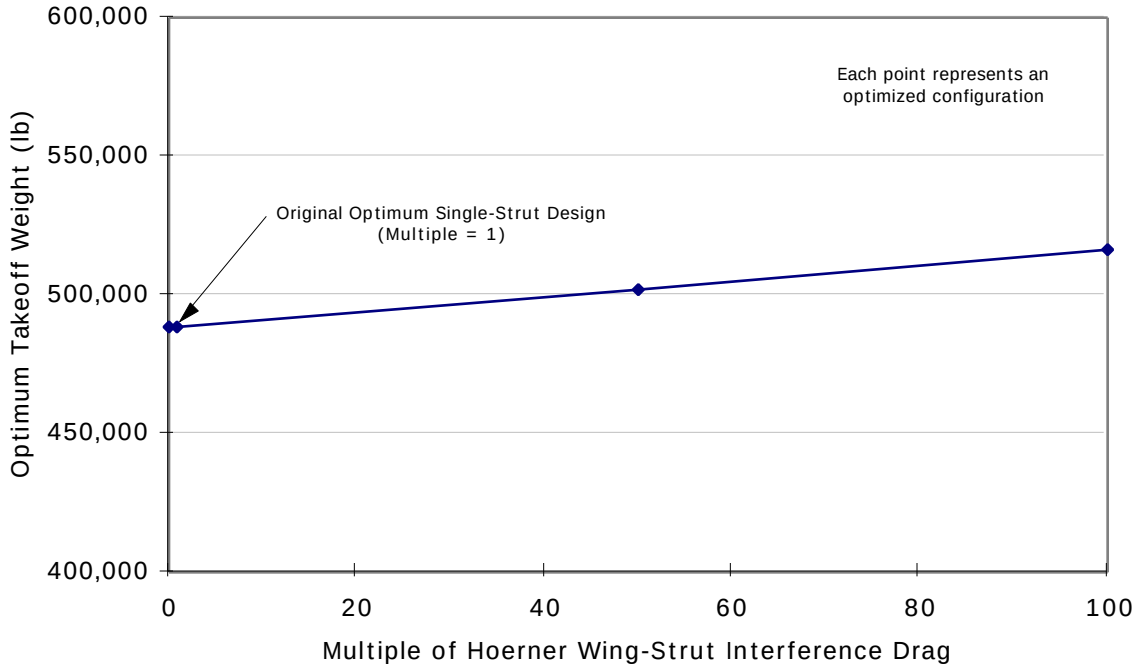

Figure 5-17: Sensitivity to the magnitude of the wing-strut interference drag

5.7. Sensitivity to the Design Mach Number

The single-strut and cantilever configurations are quite sensitive to the design Mach number, as shown in Figure 5-18. The planforms of the optimum strut-braced configurations for Mach 0.6 and 0.9 are also shown. At Mach 0.6, the optimum strut-braced configuration shows a weight savings of 55,910 lbs. (12%) over the cantilever configuration. The advantage of the strut-braced wing increases with increasing design Mach number. At Mach 0.9, the strut-braced configuration has a 82,357 lb. (14%) weight savings over the cantilever configuration.

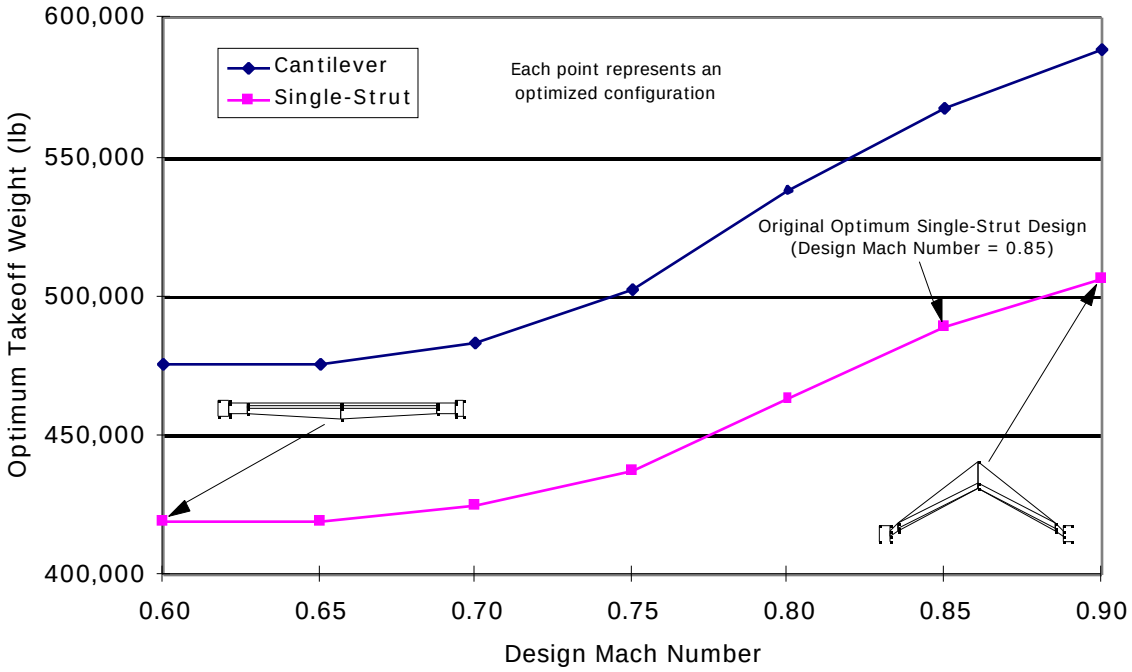

Figure 5-18: Optimum takeoff weight vs. design Mach number

6. Imagineering

In addition to the optimization studies shown above, several brainstorming sessions were held to "imagineer" innovative new design concepts. One of the most promising concepts is the arch-shaped strut. When this strut is placed in tension, it straightens out slightly and acts like a normal strut. However, instead of buckling under compression like a straight, rigid strut, it simply acts like a spring and helps to relieve the bending load. In fact, it takes at least 180˚ of rotation to actually buckle the arch-shaped strut!

The arch-shaped strut concept was utilized in the novel configuration shown in Figure 6-1. This configuration features a perpendicular intersection between the wing and struts in the front view, and a chordwise offset of the maximum thickness locations in the plan view. Both of these effects should reduce the interference drag. Additionally, the two struts complement each other by allowing one to be in tension when the other strut is likely to be in compression, thus alleviating the strut buckling problem.

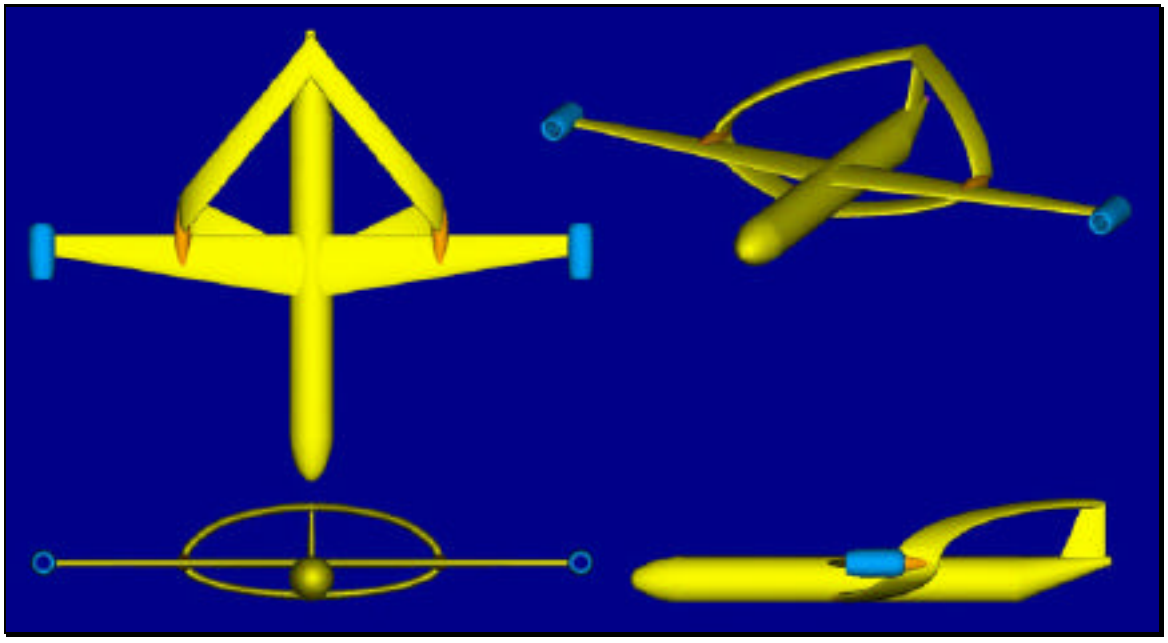

Figure 6-1: Arch-shaped strut configuration

6.1. Configuration Visualization

When performing MDO studies, it is important to provide the designer with high-quality visual feedback to communicate the shape of the configuration. To meet this goal, a Fortran subroutine was written to convert the configuration parameters of a given design into a DXF file that can be imported into AutoCAD on the PC or Infini-D on the Macintosh. These programs can then be used to create three-dimensional, rendered solid models of the configuration, animations, and virtual reality objects. An example of a rendered solid model with a background scene is shown in Figure 6-2.

Figure 6-2: Rendered solid model of the single-strut configuration

We also took the configuration visualization work one step further by creating a plastic solid model of the arch-shaped strut configuration using the *I-DEAS* solid modeling software and the rapid prototyping hardware at Virginia Tech (Figure 6-3). This technology will allow us to easily visualize complex configurations in the future.

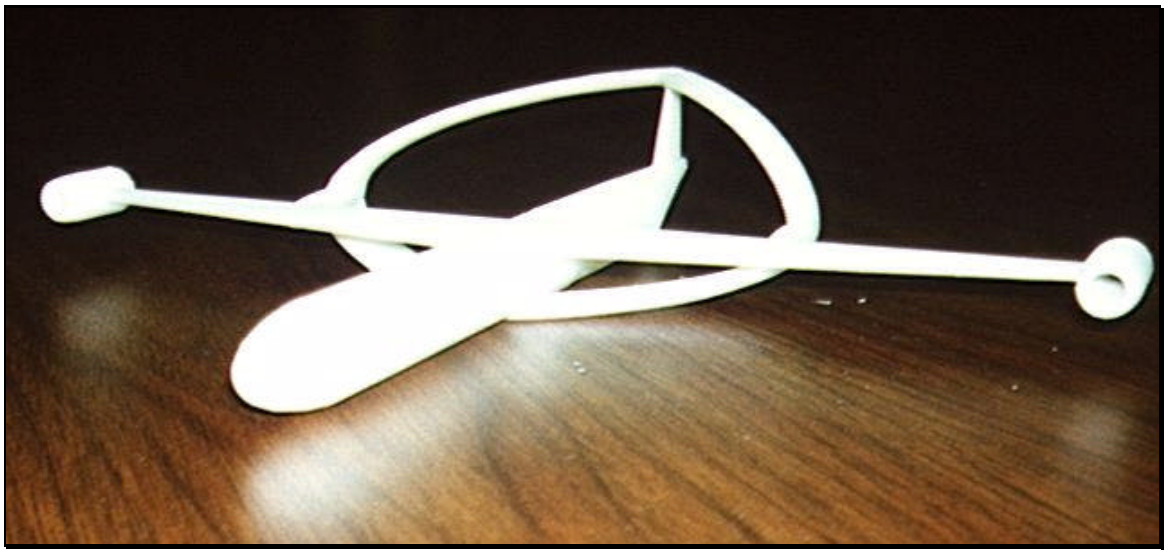

Figure 6-3: Plastic solid model of the arch-shaped strut concept

7. Conclusions and Future Work

7.1. Summary of Results

The multidisciplinary design optimization approach is absolutely essential for gaining a proper understanding of the nature of the design space and showing the true potential of a truss-braced wing configuration as envisioned by Pfenninger. Some of the results were counterintuitive at first, but more detailed investigations showed very good reasons for the design decisions made by the optimizer. For example, we initially expected the wing to unsweep to maximize the amount of laminar flow and reduce the wing weight, but the MDO method showed that the wave drag penalty for unsweeping the wing was larger than the parasite drag reduction due to the increased laminar flow and wing weight savings. Additionally, the structural analysis showed that a wing with an exceptionally small *t/c* can severely penalize the total aircraft weight and performance by dramatically increasing the wing weight.

The unique advantages of a strut-braced configuration can be best understood by tracing the design evolution from a cantilever configuration:

- The low wing weight is made possible by a novel structural concept allowing the strut to be inactive in compression, and by optimizing the strut force at the 2.5 g maneuver load condition.
- The increased structural efficiency provided by the strut can be utilized to reduce the wing weight significantly with a nearly constant span, or the span can be increased to reduce the drag with a smaller wing weight savings.
  - With tip-mounted engines, the span remains under 200 ft., and the wing weight is reduced by 30% relative to the advanced technology cantilever configuration.
  - With under-wing engines, the span is increased to 259 ft., with a wing weight reduction of 14% relative to the advanced technology cantilever configuration.
- The wing *t/c* can be reduced without a large wing weight penalty.
- The smaller *t/c* allows some unsweeping of the wing without a wave drag penalty.
- Lower weight and increased span reduce the induced drag.
- The amount of laminar flow is increased for three reasons, which reduces the parasite drag:
  - Unsweeping the wing reduces the cross-flow instability.
  - A higher aspect ratio means smaller chords and smaller Reynolds numbers.
  - Decreasing the *t/c* allows for more favorable pressure gradients and delays the shock formation.

- The taxi bump load condition imposes a natural upper limit on the span. For the tip-mounted engine configuration, the span is 198.9 ft. If the spanwise position of the engines is allowed to be a design variable, the span increases to 258.7 ft.
- According to the low-speed Hoerner interference drag equations, the wing-strut interference drag is proportional to $(t/c)^3$ and c^2, where the t/c and chord are the average values of the wing and strut. The optimum designs featured a wing and strut t/c of 5% at the wing-strut intersection, and relatively small chords. Therefore the wing-strut interference drag was predicted to be almost negligible. Future research will evaluate the transonic effects of the wing-strut intersection using CFD.

The final result is a synergistic increase in overall aircraft efficiency and a significant reduction in the takeoff gross weight, as shown in Table 7-1.

Table 7-1: Configuration summary

	Current Technology Cantilever	Advanced Technology Cantilever	SS with Tip Engines	SS with Under-Wing Engines
Wing Span (ft)	199.9	206.6	198.9	258.7
Aspect Ratio	8.7	9.8	10.3	20.5
Wing Sweep (deg)	31.6	36.7	27.3	24.5
Cruise L/D	18.8	21.7	24.4	27.8
Takeoff Gross Weight (lb)	632,081	568,031	488,990	481,236

7.2. Conclusions

The preliminary optimization studies were performed with a single-strut-braced wing, which is the most basic truss-braced configuration. The advantages relative to the advanced technology cantilever configuration are summarized in Table 7-2.

Table 7-2: Improvements of the single-strut design relative to the advanced technology cantilever configuration

	Relative to Current Technology Baseline Cantilever Configuration		Relative to Advanced Technology Optimum Cantilever Configuration	
Measure of Effectiveness	Tip Engine Design	Under-Wing Engine Design	Tip Engine Design	Under-Wing Engine Design
Takeoff Gross Weight	-23%	-24%	-14%	-15%
Fuel Weight	-36%	-42%	-21%	-29%
Operational Empty Weight	-20%	-13%	-16%	-9%
Cruise L/D	30%	48%	12%	28%
Seat-Miles/Gallon	56%	74%	26%	41%

7.3. Future Work

The large performance gains obtained by the truss-braced wing concept rely on several critical assumptions. To reduce the uncertainty associated with our results, these assumptions are being addressed in the ongoing research.

The first critical assumption is that the strut-wing interference flowfield can be controlled by modern aerodynamic design using CFD. The work to analyze and design the strut-wing juncture is currently in progress.

Another critical assumption is that good aeroelastic characteristics can be obtained without a large weight penalty. We are using NASTRAN to assess the aeroelastic properties of this class of concepts.

Both of these analysis and design efforts are computationally intense. To the extent that the results of these efforts need to be included in the MDO process, we will represent the results with response surfaces. The NASTRAN analysis will also be used to refine the wing bending material weight predictions. This will be done using response surfaces.

The truss-braced wing concept absorbs advanced concepts and technology more naturally than any other concept we've studied. Thus, we intend to assess the use of active load alleviation, active controls and tailored composite structures. Advanced arch-shaped strut configurations and multi-element truss configurations will also be investigated.

References

[1] Pfenninger, W., "Design Considerations of Large Subsonic Long Range Transport Airplanes with Low Drag Boundary Layer Suction," Northrop Aircraft, Inc., Report NAI-54-800 (BLC-67), November 1954.

[2] Smith, P.M., DeYoung, J., Lovell, W.A., Price, J.E., and Washburn, G.F., "A Study of High-Altitude Manned Research Aircraft Employing Strut-Braced Wings of High-Aspect-Ratio," NASA-CR-159262, February, 1981.

[3] Turriziani, R.V., Lovell, W.A., Martin, G.L., Price, J.E., Swanson, E.E., and Washburn, G.F., "Preliminary Design Characteristics of a Subsonic Business Jet Concept Employing an Aspect Ratio 25 Strut-Braced Wing," NASA CR-159361, Oct., 1980.

[4] Jobe, C.E., Kulfan, R.M., and Vachal, J.D., "Wing Planforms for Large Military Transports," AIAA-78-1470, 1978.

[5] Gunston, B., *Giants of the Sky: The Biggest Aeroplanes of All Time*, Patrick Stephens Limited, pp. 249-250.

[6] Patterson, J.C., and Bartlett, G.R., "Evaluation of installed Performance of a Wing-Tip-Mounted Pusher Turboprop on a Semispan Wing," NASA Technical Paper 2739, 1987.

[7] Miranda, L.R., and Brennan, J.E., "Aerodynamic Effects of Wingtip-Mounted Propellers and Turbines," AIAA-86-1802, 1986.

[8] Englar, R.J. and Williams, R.M., "Design of a Circulation Control Stern Plane for Submarine Applications," March 1971, NSRDC Tech. Note AL-200 (AD901-198), Naval Ship Research and Development Center, Bethesda, MD.

[9] Vanderplaats Research & Development, Inc., *DOT User's Manual, Version 4.20*, Colorado Springs, CO, 1995.

[10] McCullers, L.A., *FLOPS User's Guide, Release 5.81*. Text file included with the FLOPS code.

[11] Dudley, J., Huang, X., MacMillin, P.E., Grossman, B., Haftka, R.T., and Mason, W.H., "Multidisciplinary Optimization of the High-Speed Civil Transport," AIAA-95-0124, January, 1995.

[12] Grasmeyer, J.M., "Truss-Braced Wing Code Description and User's Manual," VPI-AOE-255, January, 1998.

[13] Hoak, D.E. et al., *USAF Stability and Control DATCOM*, Flight Control Division, Air Force Flight Dynamics Laboratory, WPAFB, Ohio, 1978.

[14] Grasmeyer, J.M., "A Discrete Vortex Method for Calculating the Minimum Induced Drag and Optimum Load Distribution for Aircraft Configurations with Noncoplanar Surfaces," VPI-AOE-242, January, 1997.

[15] Braslow, A.L., Maddalon, D.V., Bartlett, D.W., Wagner, R.D., and Collier, F.S., "Applied Aspects of Laminar-Flow Technology," *Viscous Drag Reduction in Boundary Layers*, AIAA, Washington D.C., 1990, pp. 47-78.

[16] Mason, W.H., "Analytic Models for Technology Integration in Aircraft Design," AIAA-90-3262, September, 1990.

[17] Malone, B. and Mason, W.H., "Multidisciplinary Optimization in Aircraft Design Using Analytic Technology Models," *Journal of Aircraft*, Vol. 32, No. 2, March-April 1995, pp. 431-438.

[18] Hoerner, S.F., *Fluid-Dynamic Drag*, published by Mrs. Hoerner, 1965. Current address: P.O. Box 65283, Vancouver, WA 98665. Phone: (206)576-3997.

[19] Roskam, J., *Methods for Estimating Stability and Control Derivatives of Conventional Subsonic Airplanes*, Roskam Aviation and Engineering Corporation, Lawrence, Kansas, 1971.

[20] Grasmeyer, J.M., "Stability and Control Derivative Estimation and Engine-Out Analysis," VPI-AOE-254, January, 1998.

[21] Mattingly, J.D., Heiser, W.H., and Daley, D.H., *Aircraft Engine Design*, AIAA, Washington D.C., 1987.

[22] Naghshineh-Pour, A.H., "Preliminary Structural Analysis of a Truss-Braced Wing," VPI-AOE-256, January, 1998.

[23] Coster, J.E., and Haftka, R., "Preliminary Topology Optimization of a Truss-Braced Wing," December 1996.

[24] Torenbeek, E., "Development and Application of a Comprehensive, Design-Sensitive Weight Prediction Method for Wing Structures of Transport Category Aircraft," Delft University of Technology, Report LR-693, Sept. 1992.

[25] Kulfan, R.M., and Vachal, J.D., "Wing Planform Geometry Effects on Large Subsonic Military Transport Airplanes," Boeing Commercial Airplane Company, AFFDL-TR-78-16, Feb. 1978.

[26] Steinbrenner, J.P., and Chawner, J.R., "The GRIDGEN Version 8 – Multiple Block Grid Generation Software", MDA Engineering, Inc., May 1993.

[27] "GASP Version 3 – The General Aerodynamic Simulation Program – Computational Flow Analysis Software for the Scientist and Engineer – User's Manual", Aerosoft, Inc., May 1996.

[28] Rosen, B.S., "Method to Predict External Store Carriage Characteristics at Transonic Speeds", NASA CR-4170, August 1988.

[29] Frink, N.T., Pirzadeh, S., and Parikh, P., "An Unstructured-Grid Software System for Solving Complex Aerodynamic Problems", NASA CP-3291, May 1995.

[30] Pirzadeh, S., "Structured background Grids for Generation of Unstructured Grids by Advancing-Fron Method", *AIAA Journal*, Vol. 31, February 1993, pp. 257-265.

[31] Pirzadeh, S., "Viscous Unstructured Three-Dimensional Grids by the Advancing-Layers Method", AIAA Paper 94-0417, 1994.

[32] Pirzadeh, S., "Three-Dimensional Unstructured Viscous Grids by the Advancing-Layers Method", AIAA Journal, Vol. 34, January 1996, pp. 43-49.

[33] Pirzadeh, S., "Progress Towards a User-Oriented Unstructured Viscous Grid Generator", AIAA Paper 96-0031, 1996.

[34] Frink, N.T., Parikh, P., and Pirzadeh, S., "A Fast Upwind Solver for the Euler Equations on Three-Dimensional Unstructured Meshes", AIAA Paper 91-0102, 1991.

[35] Sexstone, M.G., Private Communication, Systems Analysis Branch, Aeronautics Systems Analysis Division, NASA Langley Research Center, Hampton, VA 23681-0001.